

# Main anatomical characteristics of the hominin fossil humeri from the Sima de los Huesos Middle Pleistocene site, Sierra de Atapuerca, Burgos, Spain: An update

José-Miguel Carretero<sup>1,2,3</sup>  | Rebeca García-González<sup>1</sup>  | Laura Rodríguez<sup>1,4</sup>  | Juan-Luis Arsuaga<sup>3,5</sup>

<sup>1</sup>Laboratorio de Evolución Humana, Universidad de Burgos, Burgos, Spain

<sup>2</sup>Unidad Asociada de I+D+i al CSIC Vidrio y Materiales del Patrimonio Cultural (VIMPAC), Burgos, Spain

<sup>3</sup>Centro UCM-ISCIH de Investigación sobre Evolución y Comportamiento Humanos, Avda. Monforte de Lemos 5 (Pabellón 14), Madrid, Spain

<sup>4</sup>Facultad de Ciencias Biológicas y Ambientales, Departamento de Biodiversidad y Gestión Ambiental, Universidad de León, León, Spain

<sup>5</sup>Departamento de Geodinámica, Estratigrafía y Paleontología, Facultad de Ciencias Geológicas, Universidad Complutense de Madrid, Madrid, Spain

## Correspondence

José-Miguel Carretero, Laboratorio de Evolución Humana Universidad de Burgos, Edificio I+D+i-CIBA, Plaza Misael Bañuelos s/n, 09001 Burgos, Spain.  
Email: [jmcarre@ubu.es](mailto:jmcarre@ubu.es)

## Funding information

Fundación Atapuerca; Ministerio de Ciencia, Innovación y Universidades (Spain), Grant/Award Number: PID2021-122355NB-C31

## Abstract

Some of the Sima de los Huesos (SH) humeri have been previously studied and described elsewhere. Here we present an updated inventory and a review of the specimens recovered to the present day. The morphological key traits of the adult and subadult specimens are described, discussed, and illustrated. The SH humeri share with Neandertals many traits usually considered to be Neandertal specializations, thus, most of this morphological pattern is not exclusive to them. The variation found within fossil samples stresses the frequent nature of all these traits and in the specific case of the SH humeri, most of the traits considered as phylogenetically relevant are retained by their descendants, the Neandertals. Some traits are plesiomorphic for the entire genus *Homo* or are present in European hominins since the early Pleistocene. Finally, some other traits display high variability within the SH sample or different hominin samples and are of uncertain phylogenetic value. Altogether, this evidence is consistent with the hypothesis based on the overall cranial and postcranial morphology that the SH hominins are a sister group to the later Neandertals.

## KEYWORDS

arm bones, *Homo*, paleoanthropology

## 1 | INTRODUCTION AND OBJECTIVES

The Sima de los Huesos (SH) site is located well inside the Cueva Mayor–Cueva del Silo cave system, in Sierra

de Atapuerca (Burgos, Spain), and around 0.5 km from the present entrance. The site contains a bone-bearing breccia with clayish matrix mainly composed of *Ursus deningeri* as well as hominin fossils (Arsuaga et al., 1991; Arsuaga et al., 1997, 2014; Aranburu et al., 2017).

This is an open access article under the terms of the [Creative Commons Attribution-NonCommercial-NoDerivs](https://creativecommons.org/licenses/by-nc-nd/4.0/) License, which permits use and distribution in any medium, provided the original work is properly cited, the use is non-commercial and no modifications or adaptations are made.

© 2023 The Authors. The Anatomical Record published by Wiley Periodicals LLC on behalf of American Association for Anatomy.

The characteristics of this palaeoanthropological site are unusual due to the large size of the hominin accumulation corresponding to a minimum of 29 individuals, and its location far from the karst entrances (Aranburu et al., 2017; Arsuaga et al., 1997; Bermúdez de Castro et al., 2021). This fossil collection has been dated to a minimum age of 430,000 years (Arsuaga et al., 2014).

Since 1976, the SH site has yielded more than 7,000 hominin remains that we attributed to *H. heidelbergensis* (Arsuaga et al., 1991, 1997; Carretero et al., 1997) in our view, an exclusively European species ancestral only to Neandertals. This has been our position since the 1990s but we are aware that overall in the last decade, there has been recognition of the problematic nature of this designation given the large number of derived Neandertal features in the collection together with the retention of primitive features and the general lack of Neandertal features in the Mauer mandible (see, e.g., Arsuaga et al., 2014, 2015; Buck & Stringer, 2014; Manzi, 2011; Mounier et al., 2009; Stringer, 2012; Tattersall, 2011). Looking at the material from SH, *H. heidelbergensis* could acquire the identity of a European regional chronospecies in continuity with *H. neanderthalensis*, but there are reasons to place the SH material within the Neanderthal clade as a sister group to Neandertals (Arsuaga et al., 2014, 2015) rather than within *H. heidelbergensis*. Moreover, many authors (Manzi, 2011; Stringer, 2012; Tattersall, 2011) suggest the evaluation of more complex scenarios of hominin evolution in Europe than previously believed, involving either the occurrence of considerable intraspecific diversity (with archeologically distinct settlements) or, alternatively, the coexistence of different lineages (with their own respective archeological traditions) during part of the Middle Pleistocene.

Here we report the main morphological characteristics of the upper arm bone of these Middle Pleistocene hominins from the SH site. First, we update the inventory of the humeral remains recovered from SH between 1976 to the present, as well as the minimum number of individuals (MNI) represented by this bone. Some of the SH adult humeral remains have been previously partially published (Arsuaga et al., 1991, 2015; Carretero, 1994; Carretero et al., 1997, 2012, 2018) but the present work includes more complete specimens as well as, for the first time, the subadult specimens. Fieldwork at the SH site is ongoing, and the hominin fossil sample is increasing, little by little, each year.

Another objective is to review and illustrate the main morphological characteristics and their variation within the SH sample, comparing, when possible, with other fossil and recent humans to infer their possible phylogenetic significance. Main metrical variables are also provided for all SH specimens for which they are preserved and

can be reliably measured. However, we would like to caution here that our preference is for comparisons with large-bodied hominin species from Africa, Asia, and Europe (from *H. ergaster* onwards), since a very different body plan and even locomotor pattern characterizes all representatives of small-bodied *Homo* species (*H. habilis*, *H. rudolfensis*, *H. georgicus*, *H. floresiensis*, and *H. naledi*) and the australopithecines.

Finally, some palaeobiological aspects such as functional interpretations and ontogenetic variation are addressed when possible for each reported feature. We consider it to be more useful to present the description and discussion together for each anatomical trait.

## 2 | MATERIALS AND METHODS

We provide detailed images of the original specimens of SH and highlight the main anatomical features instead of reporting detailed anatomical descriptions for every specimen. We also present an inventory (Table 1 and Table 2) of the most complete specimens. We report basic measurements taken with standard anthropological techniques and instruments (Carretero et al., 1997, 1999).

The SH sample is composed of a mixed bone assemblage representing a minimum of 29 individuals of different ages and sex (Bermúdez de Castro et al., 2021). To date, only in a few exceptional occasions have bones of the same individual been associated with reasonable security (Femur-X and Pelvis 1, Carretero et al., 2004; Pelvis 1 and lumbar vertebrae, Bonmatí et al., 2010; and Cranium 5 and cervical vertebrae, Gómez-Olivencia et al., 2007; Arsuaga et al., 2015). Every recognizable fragments of hominin bone are labeled as AT-followed by the inventory number from 1 onwards (universal numbering; AT-1...AT-93...AT-4383). When several fragments (labeled with the AT-prefix) fit together, we name the new association as Humerus (abbreviated as H-) followed by a Roman numeral from I onwards (H-I...H-X...H-XX).

For comparative purposes, we have relied on measurements taken on original fossil specimens or high-quality cast (see Carretero et al., 1997 for details). For the modern human comparative samples used in assessments of adult SH individuals, we used data collected from four different samples: (a) individuals of known sex of the skeletal collection kept in the Museu e Laboratório Antropológico da Universidade de Coimbra; (b) a medieval sample of Sepúlveda (Segovia, Spain) from the Departamento de Paleontología de la Universidad Complutense de Madrid; (c) a medieval sample from the San Pablo collection housed at our laboratory at the University of Burgos, and finally (d) a sex-balanced sample of recent humans (Euroamericans and Afroamericans) from the

TABLE 1 Inventory of the adult SH humeri.

Specimen	Side	Short description
H-II	R	Complete specimen
H-III	L	Lower three-fourths of a complete bone. Proximal fracture is somewhat below the surgical neck
H-V	L	From approximately the midshaft to the upper border of olecranon fossa distally
H-VI	R	Lower three-fourths of a complete bone. Proximal fracture is around mid m. <i>pectoral major</i> insertion.
H-VII	R	Upper three-fourths of a complete bone. Distal fracture reaches almost the olecranon fossa
H-VIII	L	Lower three-fourths of a complete bone. Proximal fracture is at the top of the lateral crest of deltoid tuberosity. The central portion of the distal trochlea is missing
H-X	R	Complete specimen
H-XI	R	Lower three-fourths of a complete bone. Proximal fracture is around mid m. <i>pectoral major</i> insertion.
H-XIII	L	From the top of the lateral crest of deltoid tuberosity proximally to the middle of olecranon fossa distally. Articular surface, lateral and medial epicondyles are missing.
H-XIV	L	Lower half of a complete bone
H-XV	L	Complete specimen, although proximally the greater and lesser tubercles are badly eroded.
H-XXVI	L	Lower one-fourth of the shaft. Proximal fracture is around the minimum shaft perimeter level and distal fracture at the middle of olecranon fossa.
H-XXVII	R	Almost complete diaphysis. Proximal fracture is at the surgical neck. Distal fracture is oblique and medially includes the medial distal pillar that surrounds the olecranon fossa.
AT-93	R	Approximately, the upper half of the shaft. Upper section is somewhat above the surgical neck and distal section close to midshaft.
AT-217	R	Approximately, the lower half of the shaft. Upper fracture is close to midshaft and distal fracture is oblique and includes the medial distal pillar that surrounds the olecranon fossa
AT-464	R	Approximately, the lower one-fourth of the shaft. Proximal fracture is around the minimum shaft perimeter level and distal fracture is just above the olecranon fossa.
AT-1103	L	Almost complete proximal epiphysis up to just below the lesser tubercle.
AT-2946	L	Abraded proximal epiphysis up to around the surgical neck. The anterior portion of the head and most of the lesser tubercle is missing.
AT-2951 <sup>a</sup>	L	Distal epiphysis from the middle of the olecranon fossa level. Anteriorly, the medial border of the trochlea is missing
AT-6839	R	Distal epiphysis from the middle of the olecranon fossa level. The tip of the medial epicondyle is eroded
<i>Small fragments of diaphysis</i>		
AT-1946	?	Small fragment of the central shaft. Maximum length of 33.5 mm
AT-4049	L	Small fragment of the central shaft. Maximum length of 23.5 mm
AT-4383	R	Robust shaft fragment that includes the proximal half of the deltoid tuberosity lateral crest. maximum length of 61.5 mm
<i>Small fragments of proximal epiphysis</i>		
AT-2580	R	Humeral head fragment
AT-4023	L	Humeral head fragment
AT-4024	L	Humeral head fragment
AT-4026	R	Medial half of the humeral head. Maximum breadth can be measured = 49 mm
AT-4027	R	Tip of the greater tubercle and bicipital sulcus
AT-4221	?	Humeral head fragment
<i>Small fragments of distal epiphysis</i>		
AT-268	R	Fragment of medial epicondyle and the medial lip of the trochlea
AT-333	R	Central portion of the trochlea

(Continues)

TABLE 1 (Continued)

Specimen	Side	Short description
AT-1781	R	Fragment of medial epicondyle and the medial lip of the trochlea

Note: Composition of specimens: H-II = AT-787 + 788 + 1115; H-III = AT-661 + 1114; H-V = AT-1094 + 1102; H-VI = AT-1112 + 1113 + 1691; H-VII = AT-1107 + 2052 + 5142; H-VIII = AT-3493 + 3494; H-X = AT-25 + 4315; H-XI = AT-1110 + 2046; H-XIII = AT-4184 + 4170; H-XIV = AT-790 + 2097; H-XV = AT-658 + 2468 + 4316; H-XXVI = AT-6849 + 6850; H-XXVII = AT-6680.

<sup>a</sup>Specimen comprised by AT-2951 + 2952.

TABLE 2 Inventory of the subadult SH humeri.

Specimen	Side	Short description
H-I	R	Abraded small distal epiphysis.
H-IV	L	Complete left specimen except for the humeral head. Proximal metaphyseal surface as well as the distal epiphysis are well preserved. Medial epicondyle was not fused
H-IX	R	Proximal half of the humerus.
H-XII	L	Approximately distal two-thirds of the bone. From the distal portion of the bicipital sulcus to the distal end from which the central portion is missing. The medial epicondyle, trochlea nor capitulum were fused.
H-XVI	L	Approximately proximal two-thirds of the bone.
H-XVII	R	Complete bone from proximal to distal metaphysis. Distal end has lost some fragments. The medial epicondyle, trochlea nor capitulum were fused.
H-XVIII	L	Diaphysis from the roof of the olecranon fossa to approximately the middle of the deltoid tuberosity.
H-XIX	R	Central part of the diaphysis from the supraolecranon level to the beginning of the bicipital sulcus.
H-XX	L	Fragmented diaphysis from the supraolecranon level to the middle of the deltoid tuberosity.
H-XXI	L	Fragmented diaphysis from the supraolecranon level to the middle of the deltoid tuberosity.
H-XXII	L	Distal third of the bone only preserves the epicondylar region.
H-XXIII	L	Approximately central one-third of the diaphysis
H-XXIV	R	Almost complete bone. From proximal metaphysis to an eroded olecranon fossa. Medial pillar is missing
H-XXV	R	Approximately distal third of the diaphysis with the olecranon fossa roof and portions of lateral and medial pillars
H-XXVIII	L	Proximal one-third of the humerus. Includes part of the metaphysis and the bicipital region.
H-XXIX	R	Central portion of the diaphysis
AT-69	R	Small fragment of distal diaphysis just above olecranon fossa.
AT-740	R	Complete isolated and unfused capitulum and lateral part of the trochlea (distal lateral ossification center).
AT-789	L	Eroded proximal portion of the bone. Most of the metaphyseal surface is missing.
AT-1089	L	Approximately proximal one-fourth of the specimen. From metaphyseal surface to the end of bicipital sulcus
AT-1117	R	Complete distal articular surface and part of the olecranon fossa. Medial epicondyle was not fused
AT-1787	R	Complete and well-preserved unfused humeral head
AT-1801	L	Eroded unfused humeral head
AT-1821	R	Complete isolated and unfused capitulum and lateral part of the trochlea (distal lateral ossification center).
AT-1967	L	Eroded unfused humeral head
AT-2568	L	Complete isolated and unfused capitulum and lateral part of the trochlea (distal lateral ossification center).
AT-3986	L	Eroded unfused humeral head
AT-4499	R	Eroded distal articular surface
AT-5409	L	Eroded unfused humeral head
AT-5635 <sup>a</sup>	L	Eroded unfused humeral head

Note: Composition of specimens: H-I = AT-741 + 791; H-IV = AT-1084 + 1108 + 1116; H-IX = AT-1101 + 1813; H-XII = AT-1096 + 2200 + 2431; H-XVI = AT-2204 + 2574; H-XVII = AT-1095 + 4095 + 4699; H-XVIII = AT-4175 + 4625 + 5605; H-XIX = AT-660 + 4180 + 4181; H-XX = AT-4167 + 4169 + 4503; H-XXI = AT-2563 + 2564; H-XXII = AT-1269; H-XXIII = AT-1268; H-XXIV = AT-1808; H-XXV = AT-322 + 2357; H-XXVIII = AT-2123 + 4783; H-XXIX = AT-742 + AT-1999.

<sup>a</sup>Specimen comprised by AT-5635 + 5636 + 5637 + 5638 + 5684. In addition to the present inventory, there are some more recognized specimens with still little anatomical information: four small fragments of proximal epiphysis, 12 fragments of central portions of diaphysis between 50 and 109 mm in length, and 25 bone flakes.

Hamann–Todd Collection housed in the Cleveland Museum of Natural History (Ohio). Also, literature references to these and other samples are used in the comparisons and quoted within the text.

Descriptions of the traits are mainly based on adult specimens but subadult conditions are also reported when possible. The age at death of isolated bones of fossil species is difficult to assess and, in most cases, just the mature or immature status is indicated. Nevertheless, as metric and morphological traits change with age, a precise determination of age at death is very important for comparisons among immature specimens in order to avoid misinterpretations. The maximum humeral intermetaphyseal length (HIL) is a very useful variable for properly estimating age at death in modern subadult individuals, and there is one specimen from SH that preserves this unaltered dimension, Humerus XVII. Nevertheless, we are aware that the predictive models for estimating age at death based on modern children have limitations when applied to fossil specimens (i.e., inter- and intra-specific variation in patterns of growth and development, variation in body size and body proportions, etc.). In order to partially overcome these problems, we estimate the age at death of this SH specimen (H-XVII) from predictive equations derived from 11 modern samples with different growth patterns, body sizes, and proportions (Table 3). Ten out of these 11 formulae were developed by least squares regression and inverse calibration model (age is the dependent variable regressed on HIL). The authors have previously applied this approach in Bermúdez de Castro et al. (2012) to estimate the age at death of the ATD6-121

subadult humerus of *Homo antecessor*, a lower Pleistocene species. Nevertheless, the classical calibration (HIL is regressed on age followed by a solution for the age) is preferred if it is suspected that the estimated ages will be an extrapolation beyond the useful limits of the reference sample ages (Konigsberg et al., 1998). Thus, to cover as much recent variation and as many methodological approaches as possible, we have also employed here the classical calibration model proposed by Cardoso et al. (2014) (formula no. 11 in Table 3). A weighted mean age and its 99% confidence limit are calculated for the SH H-XVII specimen via meta-analysis (the age derived from each regression equation is treated as an individual case, so the standard error of the estimation for each regression formula is incorporated in the final calculation).

There are within the SH sample other immature specimens whose distal epiphyses are already fused or are in the process of fusing. In these cases, we have used established chronological standards for the union of the epiphyses and diaphysis to estimate age (Cardoso, 2008). Finally, for the isolated proximal and distal epiphyseal remains we have also used the standard charts of changes in shape and size with age of these epiphyses (Brodeur et al., 1981).

Following the estimation of age at death, comparisons of metric and morphological traits in the subadult SH individuals were made with the appropriate age groups. In this case, for comparison used in assessments of subadult SH individuals, we use three recent hominin collections of individuals with known age at death: (a) the sample housed in the Bocage Museum (National

**TABLE 3** Age (in years) prediction regression formulae used for subadult individuals.

No.	Sample	N	Equation	R <sup>2</sup>	SEE/MSE
1	Spitalfields <sup>a</sup>	90	Age = -5.09 + 0.06 + HIL	.91	0.92
2	Portuguese <sup>a</sup>	48	Age = -4.92 + 0.07 + HIL	.77	2.11
3	HTH <sup>a</sup>	18	Age = -4.91 + 0.06 + HIL	.61	1.85
4	San Pablo <sup>a</sup>	25	Age = -6.03 + 0.07 + HIL	.86	1.01
5	Dart <sup>b</sup>	42	Age = -5.46 + 0.07 + HIL	.86	1.43
6	Kulubnarti <sup>b</sup>	61	Age = -7.25 + 0.08 + HIL	.82	1.57
7	Mistihalj <sup>b</sup>	29	Age = -10.50 + 0.09 + HIL	.88	1.55
8	Indian Knoll <sup>b</sup>	72	Age = -8.74 + 0.09 + HIL	.92	1.34
9	California <sup>b</sup>	70	Age = -7.94 + 0.08 + HIL	.93	1.25
10	Point Hope <sup>b</sup>	61	Age = -7.64 + 0.08 + HIL	.89	1.31
11	Portuguese <sup>c</sup>	102	Age = (HIL-79.97)/13.51	.92	1.13

Abbreviations: HIL, humeral intermetaphyseal length (in mm); MSE, mean standard error; SEE, standard error of estimate.

<sup>a</sup>From Bermúdez de Castro et al. (2012).

<sup>b</sup>From Cowgill (2007). Formulae developed for individuals 3 years of age and older.

<sup>c</sup>From Cardoso et al. (2014). Formulae developed for individuals 2 years of age and older.

Museum of Natural History, Lisbon, Portugal), (b) the sample housed in the Department of Life Sciences at Coimbra University (Coimbra, Portugal), and (c) a sample derived from the Hamann-Todd collection (HTH) housed in the Cleveland Museum of Natural History (Ohio, USA). In order to cover a larger range of variation, the three subsamples were pooled in a larger single sample of recent humans. It is also important to note that in some age groups, there are both individuals with a fused distal epiphysis and others without. To take into account this aspect, we divided these age groups into two different subgroups: one with distal epiphyses unfused and one with distal epiphyses fused.

### 3 | RESULTS AND DISCUSSION

#### 3.1 | Inventory and minimum number of individuals

A large number of humeral specimens have been recognized to date from SH. Among the adults, there are three complete bones (H-II, H-X, and H-XV) and another 29 specimens that represent different portions of the bone in variable states of preservation (Table 1). Among the immature remains, there are four virtually complete specimens (H-IV, H-XII, H-XVII, and H-XXIV), all of them lacking only the still unfused proximal and/or distal epiphysis. In addition to these, another 26 partial bones have been recovered, including several isolated unfused epiphyses (Table 2). Tables 4, 5, and 6 contain the main dimensions of the most complete adult humeri. The main dimension and comparative data for the most complete subadult humeri are presented in Table 7.

Main subadult specimens are illustrated in Figures 1–5, and figures of the main adult specimens can be found sorted by specimen number in Figures 15–24. Additional views of specimens are also figured throughout the text as necessary.

Eight is the MNI represented by adult humeri based on incompatible distal epiphyses of the right side

(complete or partial). Seven are represented by the distal epiphysis of the left side. Additionally, seven is also the MNI represented by immature specimens based on incompatible distal regions of both the right and left sides. Thus, at least 15 different individuals are represented by the humeri within the SH sample, eight adults, and seven subadults.

#### 3.2 | Age at death of the subadult individuals

Regarding the isolated unfused proximal epiphyses, all of them show the same maturation stage in which, although unfused, they resemble the fully adult morphology (Figure 1). AT-1801 and AT-1787 are good examples to represent this maturity stage. In these examples, both the greater and lesser tubercles are well-defined, and the articular surface appears smooth and without pitting, while the metaphyseal surface is hollowed and billowed. In recent humans, this stage in which the epiphysis is mature but unfused occurs during adolescence. At present, it is not possible to associate any proximal epiphyses to a specific diaphysis, and therefore, the age at death of these specimens cannot be estimated more accurately.

The developmental sequence represented by the ossification centers of the distal epiphysis is more complete than that of the proximal end. The isolated centers of capitula AT-1821 and AT-2568 represent the first detected developmental stage (Figure 2). These two specimens are almost spheric, but they have not developed the complete curvilinear outline typical of adults (Brodeur et al., 1981). In recent humans, the curvilinear outline of the capitulum is noted as early as 5.5–6.0 years but can be absent up to its latest appearance at 9–9.5 years. Thus, we only can say that these SH capitula are under 9.5 years. AT-740 represents the next developmental stage of this ossification center in which the lateral part of the trochlea is already formed (Figure 2). Following recent hominin standards, this stage occurs around 12 years (Brodeur et al., 1981).

TABLE 4 Main dimensions and indices of the adult SH humeral proximal epiphysis (in mm).

Proximal epiphysis Side	H-II R	H-VII R	H-X R	H-XV L	AT-1103 L	AT-2946 L	AT-4026 R	Mean ± SD; N
Proximal epiphysis breadth	50.7	51.1	51.7		45.7	48.2		49.5 ± 2.5; 5
Head vertical diameter	44.7	43.3	43.5	42	38.9			42.5 ± 2.2; 5
Head transverse diameter	47	48.5	48	(44)	41	43.1	49	45.8 ± 3.1; 7
Head shape index	105.1	112	110.3	104.8	105.4			107.5 ± 3.4; 5

Note: Parentheses indicate estimated value. Head shape index = (Head transverse diameter/Head vertical diameter) × 100.

TABLE 5 Main dimensions and indices of the adult SH humeral diaphysis (in mm).

Diaphysis Side	H-II	H-III	H-V	H-VI	H-VII	H-VIII	H-X	H-XI	H-XIII	H-XIV	H-XV	AT-93	AT-217	Mean ± SD; N
	R	L	L	R	R	L	R	R	L	L	L	R	R	
Maximum length	342						318				342			334 ± 13.9; 3
Midshaft maximum diameter	25	23.6	22	22.7	25.8	23.9	24.5	17.6	17.5	20.2	22	27.6	25	22.9 ± 3.0; 13
Midshaft minimum diameter	19.1	18.2	16.5	16.5	20.3	18	18.8	13	14.2	16	15.2	19	21	17.4 ± 2.4; 13
Midshaft index	76.4	77.1	75	72.7	78.7	75.3	76.7	73.8	81.1	79.2	69.1	68.8	84	76 ± 4.3; 13
Midshaft perimeter	71	67	62	65	75	68	70	53	53	58	62	79	74	65.9 ± 8.1; 13
Minimum shaft perimeter	70	66		64	74	67	69	52	52	57	60		74	63.7 ± 7.7; 11
Robusticity index	49.3						21.7				17.5			29.5 ± 17.3; 3
Retroversion angle (°) <sup>a</sup>	35						48				36			39.7 ± 7.2; 3

Note: Midshaft index = (Midshaft minimum diameter/Midshaft maximum diameter) × 100. Robusticity Index = (Minimum shaft perimeter/Maximum length) × 100.

<sup>a</sup>Although complementary, we give here both retroversion and torsion angles.

Regarding the epiphyseal fusion sequence, in the SH sample, there are two different developmental stages represented. H-XII and H-XVII (Figure 3) represent the first stage in which there is no trace of distal epiphysis fusion. Nevertheless, this only provides a maximum age of 16 years if they belong to a male individual or 14 years if they belong to a female individual (Cardoso, 2008). Fortunately, H-XVII is complete, and we can estimate its age at death based on the humeral intermetaphyseal length (HIL, see the previous section and Table 7). Our meta-analysis provides a mean age of 10.3 years with a 99% confidence interval between 9.33 and 11.3 years. Moreover, the isolated capitulum AT-1821 (see above) fits well with the distal metaphysis of H-XVII. Considering the maximum age at death estimated for this capitulum (under 9.5 years old), it is reasonable to infer an age at death between 9.5 and 10 years old for H-XVII (Table 7). The less complete H-XII from the left side shares with H-XVII (right side) the distal end dimension and some anatomical details such as muscular impressions that suggest that they could belong to the same individual.

H-IV (Figure 4) represents the other developmental stage where the distal compound epiphysis is fused, but the medial epicondyle remains unfused. Although H-XXIV (Figure 4) is broken at its distal end, some traces of distal fusion are visible. Thus, following recent hominin standards, the age estimated for H-IV and H-XXIV is between 11 and 16 years (Table 7). However, H-IV is shorter than H-XXIV so it is unlikely that they belong to the same individual. The age at death of these seven postcranial individuals is congruent with those of the 12 subadult individuals identified by dental remains (Bermúdez de Castro et al., 2021). In addition to these, there are 13 other subadult humeral fragments whose age at death is uncertain and quite difficult to establish (Figure 5).

### 3.3 | Main metric and morphological features of the SH humerus

#### 3.3.1 | Maximum length

Maximum length is quite variable within recent human populations (Delsaux, 1977; Vandermeersch & Trinkaus, 1995) as well as among the three complete SH specimens (Carretero et al., 1997). H-II and H-XV can be considered long humeri (maximum length = 342 mm; more than 2.5 SD above many reported recent samples). On the contrary, H-X has a maximum length (318 mm) that is more common among recent humans. The small available Neandertal sample is characterized by a

TABLE 6 Main dimensions and indices of the adult SH humeral distal epiphysis (in mm).

Distal epiphysis SIDE	H-II		H-III		H-VI		H-VIII		H-X		H-XI		H-XIV		H-XV		AT-2952		AT-6839		H-XXXVI		AT-6903		Mean $\pm$ SD; N
	R	L	R	L	R	L	R	L	R	L	R	L	R	L	R	L	R	L	R	L	R	L	R	L	
Maximum biepicondylar breadth	65	66	61	56.7	63.1	56.7	56.2	61.1	(61.0) <sup>a</sup>	(60–61) <sup>b</sup>															61.2 $\pm$ 3.3; 9
Distal articular breadth	47	47.9	45.5	42	46.2	42	43.5	45	46.0	45.1															45.4 $\pm$ 1.8; 9
Distal articular breadth index	72.3	72.6	74.6	74.1	73.2	74.1	77.4	73.6	75.4	74.5															74.2 $\pm$ 1.7; 8
Trochlear breadth	29	29	30	27	27	24.8	27	26.2	28.4	26.3															27.5 $\pm$ 1.7; 9
Capitulum height	19.5	20.7	17	17	18.9	17	17	19.1	17.9	17.6															18.3 $\pm$ 1.3; 9
Capitulum breadth	18.2	19	16	17.5	17	17.5	15.7	16.8	16.0	16.8															17.0 $\pm$ 1.1; 9
Capitulum shape index	93.3	91.8	94.1	102.9	89.9	102.9	92.4	88.0	89.4	95.5															93.0 $\pm$ 4.4; 9
Medial epicondyle thickness	16.0	16.0	14.8	13.5	14.5	13.5	12.2	12.8	14.5																14.6 $\pm$ 1.6; 9
Olecranon fossa breadth	30	34	30	32	29.6	32	27	29	29.1	(30.0) <sup>c</sup>															30.4 $\pm$ 2.0; 9
Distal medial pillar thickness	10	9	8.4	7.8	10.5	7.8	7.0	6.5	7.5																8.6 $\pm$ 1.5; 10
Distal lateral pillar thickness	16.9	16.5	17.6	12	15.1	12	13	10.6	12.3																14.9 $\pm$ 2.0; 8
Medial pillar index	15.4	13.6	13.8	13.8	16.6	13.8	10.6	10.6	12.3																13.7 $\pm$ 2.0; 7
Lateral pillar index	26.0	25.0	28.9	21.2	23.9	21.2	24.9	21.3																	24.4 $\pm$ 2.7; 7

Note: Parentheses indicate estimated values. Distal articular breadth index = (Distal articular breadth/Biepicondylar breadth)  $\times$  100 (Carretero et al., 1997). Capitulum shape index = (Capitulum breadth/capitulum height)  $\times$  100 (Carretero et al., 1997). Medial pillar Index = (Medial pillar thickness/Biepicondylar breadth)  $\times$  100 (Carretero et al., 1997). Lateral pillar Index = (Lateral pillar thickness/Biepicondylar breadth)  $\times$  100 (Carretero et al., 1997).

<sup>a</sup>The lateral epicondyle is not preserved in this specimen and the maximum preserved biepicondylar breadth is 59.6 mm. The actual biepicondylar breadth could be 1 or at most 2 mm larger, so we think that 61 mm is very reasonable.

<sup>b</sup>In this case, the maximum preserved biepicondylar breadth is 59.2 mm as the medial epicondyle is not complete (Figure 15). Judging from other specimens from SH of the same distal articular size, the biepicondylar breadth of AT-6839 should be about 60 or 61 mm. We have adopted 60.5 mm to compute the distal articular breadth index.

<sup>c</sup>With a minimum of 28.5 mm, we have added 1.5 mm due to the abrasion of the posterolateral surface.

TABLE 7 Main dimensions of the most complete subadult humeri from SH and some comparative recent data.

Side Preservation	H-IV	H-XII	H-XVII	H-XXIV	Recent age groups for comparisons					
	L	L	R	R	9–11		12–16 unfused		12–16 fused	
	Complete	Partial	Complete	Partial	(N = 23)		distal end (N = 11)		distal end (N = 8)	
Estimated age at death (years)	11–16	9.5–10	9.5–10	11–16	Mean	SD	Mean	SD	Mean	SD
Variables					Mean	SD	Mean	SD	Mean	SD
Humeral length	270	233 <sup>a</sup>	233	293 <sup>b</sup>	203.0	31.2	249.7	27.5	287.1	29.2
Midshaft min. diameter	15.2	13.4	12.8	16.1	12.7	1.5	14.0	1.2	16.0	1.2
Midshaft max. diameter	18.8	17.2	14.9	20.1	14.8	1.6	16.7	1.4	19.0	1.9
Midshaft perimeter	54	60	50	60	45.3	5.8	50.4	5.2	32.8	19.7
Distal metaphyseal breadth (DMB)	52.0	48.0			38.7	3.8	44.8	5.7	49.9	10.3
Olecranon fossa breadth (OFB)	28.3	25.5			19.9	2.5	25.4	8.2	29.9	8.2
Medial pillar thickness (MPT)	8.3	9.2			7.9	1.1	11.0	3.6	13.8	4.3
Lateral pillar thickness (LPT)	14.9	13.4			11.9	1.9	13.7	1.9	15.4	2.0
Midshaft index	80.8	77.9	85.9	89.1	85.8	4.1	83.9	4.3	84.2	9.4
Robusticity index	20.0	(25.7)	21.5	(20.5)	22.7	3.7	19.5	5.7	11.8	7.5
Pillar index	55.7	68.7			67.6	10.5	77.3	24.3	90.4	29.2
MPT/DMB	16.0	19.2			20.4	2.0	25.0	6.4	29.0	11.0
MPT/OFB	29.3	36.1			40.1	5.6	45.2	7.4	45.2	7.4
OFB/DMB	54.4	53.1			51.2	3.4	55.7	12.4	55.7	12.4
DMB/Humeral length	19.3	(20.6)			19.4	2.8	18.0	1.8	17.1	3.7
Retroversion angle	35°		59.6°							

<sup>a</sup>Humeral length assuming that the specimen belongs to the same individual as the complete H-XVII. In parentheses, the computed values assuming that humeral length.

<sup>b</sup>Maximum preserved length is 288 mm. We have estimated the maximum length of H-XXIV by rescaling and joining in 3D images from CT-Scan of the distal epiphysis AT-1117 that is in a compatible state of development. In parentheses, the computed robusticity index assuming this humeral length.

comparatively short humerus ( $301.6 \pm 12.0$ ,  $n = 6$ ; Carretero et al., 1997). It is unclear at present whether within this population the variation in SH humerus length is related to high variation in arm proportions or brachial index. For this, it is necessary to associate humeri and radii which is still difficult to accomplish with certainty. In sum, the present sample from SH indicates that these hominins were quite variable in humeral length and that, probably, on average they were above the values that characterized the later Neandertals.

### 3.3.2 | Midshaft shape

The shape of the humeral shaft, as expressed by the midshaft index (Table 5), is also quite variable in recent

humans, and rounded shafts and mediolaterally compressed shafts are each observed in nearly 50% of the samples (Aiello & Dean, 1990; Delsaux, 1977). Among the SH hominins, all shaft morphotypes are also represented, and both, mediolaterally compressed and rounded midshafts are each observed at a frequency of approximately 50% in the adult total sample. Six out of 13 adult specimens have a shaft index within the platybrachic range, that is, mediolaterally compressed shaft or a midshaft index below 76.5. H-II is near this limit (76.4). The other six adult specimens exhibit eurybrachia (i.e., rounded midshaft or an index above 76.5; Table 5). The SH mean is also very close to the platybrachia limit ( $75.9 \pm 4.4$ ). Finally, all subadult humeri are characterized by eurybrachia (Table 7). The same variation can be found in the Neandertals (Delsaux, 1977; Thoma, 1975;

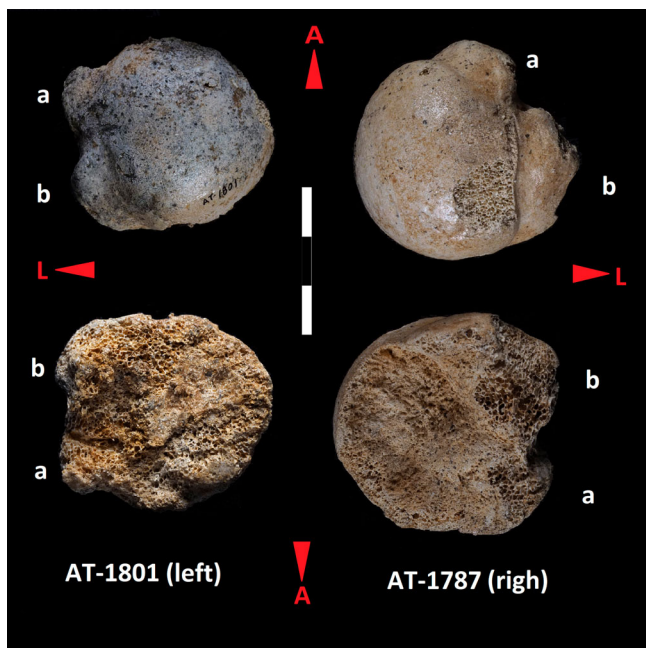


**FIGURE 1** Proximal unfused epiphysis AT-1801 (left side) and AT-1787 (right side) in proximal (above) and metaphyseal (below) views. All subadult proximal epiphyses from SH show the same maturation stage. AT-1801 and AT-1787 are good examples of this stage where they resemble the adult ones. Both, the lesser (a) and greater (b) tubercles are well-defined and easily identifiable. The articular surface appears smooth without pitting (above), while the metaphyseal surface is hollowed and billowed (below). Scale in cm

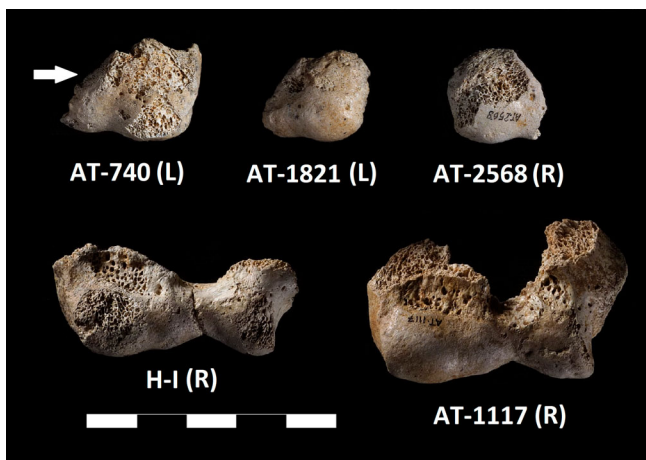


**FIGURE 2** Subadult distal epiphyseal remains in different states of development. *Top row*: three complete isolated unfused capitula and lateral part of the trochlea (distal lateral ossification center). AT-1821 and AT-2568 are a left and right capitulum which represents the first developmental stage where the trochlea is barely present. AT-740 (left side) represents the following stage in which the lateral part of the trochlea is already formed (white arrow). *Bottom row*: anterior view of two distal epiphyses that represent the last stage of development where only the medial epicondyle has not yet been merged, although H-I is likely younger than AT-1117. R, right humerus; L, left humerus. Scale in cm



**FIGURE 3** Subadult left H-IV and right H-XXIV in anterior and posterior views from left to right. Scale in cm



**FIGURE 4** Subadult left H-XII and right H-XVII in anterior and posterior views from left to right. Scale in cm

Trinkaus, 1983; Vandermeersch, 1991), though most of the specimens are characterized by platybrachia (82%,  $n = 22$ ).

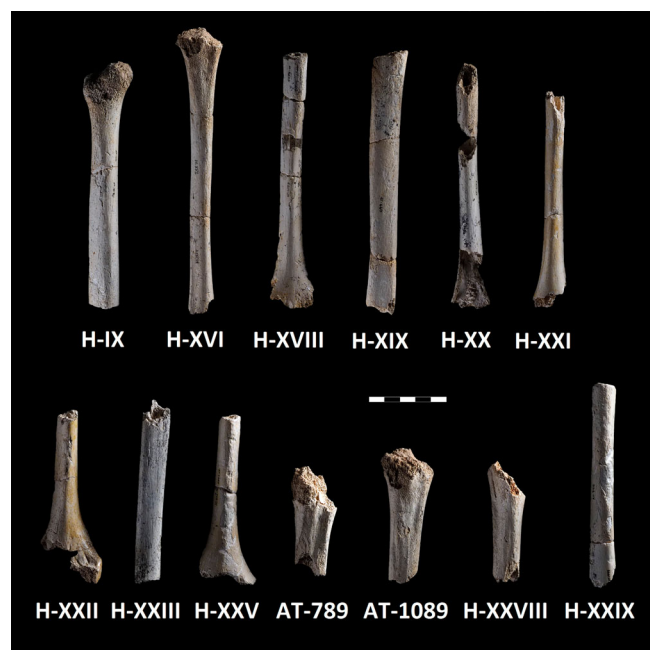


FIGURE 5 Other humeral subadult specimens from SH in anterior view. R, right humerus; L, left humerus. Scale in cm

### 3.3.3 | Robusticity index and handedness

Among the three complete SH humeri, the robusticity index varies considerably (from 49.3 to 17.5; Table 5). This index is higher in H-II (49.3) and H-X (21.5), both from the right side, than in H-XV (17.5), which is the same length as H-II but is from the opposite side. The shaft robusticity variation could be related to arm laterality, a condition that it is common among recent humans and Neandertals (Auerbach & Ruff, 2006; Pérez-Criado et al., 2017; Ruff et al., 1993; Sládek et al., 2016; Trinkaus et al., 1994). Nevertheless, while the humeral shaft asymmetry can be very large, asymmetry in humeral length and articular breadth, although favoring the right side, is relatively small and consistent between temporal periods (Sládek et al., 2016).

Fitting into this pattern, the differences in shaft dimensions between H-II and H-XV are quite large, while the proximal and distal articular dimensions are more similar. These differences could be attributed to laterality within the same individual, as they are similar to articular laterality differences found among different Pleistocene and recent *H. sapiens* samples (Sládek et al., 2016; Trinkaus et al., 1994). Nevertheless, H-III, also from the left side but incomplete, is very similar in morphology, shaft, and articular dimensions to H-II and a perfect candidate to be its antimere. In this case, laterality would not be significant. In any case, as we have detected in previous studies, the humeral shaft laterality could play an important role in the variation of SH sample (Arsuaga

et al., 1997, 2015; Lorenzo et al., 1998). Diaphyseal cross-sectional parameters of Neandertal humeri are always larger on the right than on the left side, which is interpreted as a sign of right-hand dominance (Trinkaus et al., 1994). Although we cannot be certain of the association of bones from the same individual, we found the same bias in the SH sample favoring right side.

The subadult complete H-IV and H-XVII show a robusticity index close to the mean of their respective age groups (12–16 and 9–11). However, it is important to note that H-IV already has the distal epiphysis fused and compared to our recent subgroup in the same condition, this SH specimen is a robust bone (1 SD above the recent mean of 12–16 years with fused distal end; Table 7). The same is true if we consider the estimated length for H-XXIV: its robusticity index is 1 SD above the mean of the group with fused distal epiphyses.

Interestingly, H-IV is from the left side and our recent sample is not divided by side. In this sense and as mentioned above, H-XII (incomplete) and H-XVII could belong to the same individual, but the shaft dimensions of the former (left side) are larger than those of the latter (right side). Assuming the same length for both specimens (233 mm), the robusticity index of H-XII (25.7) is higher than in H-XVII (21.5) albeit just moderately high compared with our recent sample (0.8 SD above the recent sample mean of 9–11 years; Table 7). These differences in shaft dimensions are equivalent to those we found between the adult specimens H-II (R) and H-XV (L), but in the opposite direction (in the subadult the left side is the most robust). Since there is no reason to discard laterality as an explanation for some robusticity variation among the subadults, and assuming that H-XII and H-XVII belong to the same individual, the humeral shaft asymmetry manifests itself early in life in this Pleistocene population.

In the SH sample, handedness has been studied by analyzing incisor labial striation and brain endocast asymmetries (Lozano et al., 2009; Poza-Rey et al., 2017). A left-handed preference was inferred for subadult Cranium-16 based on both dental striations and endocranial petalias (i.e., greater protrusion of one cerebral hemisphere relative to the other). On the other hand, another subadult cranium (Cr-6) was inferred to have a left-handed preference based on endocranial asymmetries, however, the handedness inference based on dental striae does not coincide (Poza-Rey et al., 2017). One possibility contemplated by these authors is that this individual was ambidextrous. The estimated dental ages for Cranium-6 (13.3–16.1 years old) and Cranium-16 (16–17 years old) are older than those obtained for H-XII and H-XVII (9.5–10 years old; Table 7). However, it is important to note that the dental age was estimated from the

development of the third molar and Modesto-Mata et al. (2022) have shown that SH hominins show an advanced development of the third molars with respect to the recent *Homo sapiens*. This fact, combined with the reduced enamel formation times, indicates a shorter dental development pattern in comparison to recent hominin averages. Thus, it is likely that dental age in these hominins is overestimated when we use modern dental standards. In any case, the possible humeral asymmetry detected between the H-XII and H-XVII (if they belong to the same individual) is compatible with the evidence of handedness found within the SH subadult crania.

### 3.3.4 | Cross-sectional parameters

Cross-sectional parameters of the humeral shaft can also be studied at 35% humeral length (below mid-shaft) within the SH sample (Carretero et al., 2009; Rodríguez, 2013). First, generalized thickening of cortical bone is a well-known postcranial characteristic of SH (Carretero et al., 2009) and other archaic hominins (Churchill, 1998; Di Vincenzo et al., 2015; Trinkaus et al., 1994, 1999; Trinkaus & Churchill, 1999). We think that this trait could characterize not only limb bones, but the entire skeleton of SH hominins (Carretero et al., 2018). The relatively thicker cortical bone demonstrates the greater resistance of all these archaic humeri to axial loading in comparison with some recent humans (Trinkaus & Churchill, 1999). According to Trinkaus et al. (1999), at both the 35% and 65% levels, Neandertals generally have a higher relative cortical area than early recent humans, and the SH hominins share this pattern with Neandertals (Arsuaga et al., 1991, 2015, Rodríguez, 2013; Figure 6).

Other cross-sectional geometric parameters measure the distribution of skeletal tissue in bone sections and provide biomechanically relevant measurements that reflect loading modes, structural adaptation, and activity

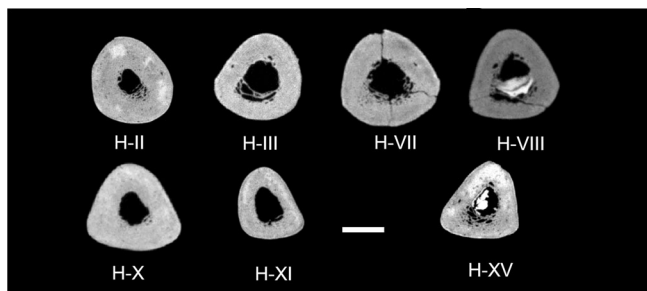


FIGURE 6 Cross-sections at 35% of the total length of some humeri from SH. Sections are view from distal and in all of them anterior is up. Scale represents 1 cm

patterns (e.g., Katzenberg & Saunders, 2008; Larsen, 1997; Ruff, 2000, 2008). Analysis of the polar moments of area of SH humeri at 35% of their maximum length (Rodríguez, 2013), indicates that, when size (humeral length) is considered, the moments of inertia  $I_x$  and  $I_y$  (bone distribution) do not differ significantly from those of some medieval samples on either side, reflecting similar levels/patterns of activity. As proposed by Larsen et al. (1995) and Trinkaus and Churchill (1999), since the polar moments of area combine the effects of cortical area and the relevant distribution of bone within the cross-sections, the comparisons of these parameters with humeral length provide a better evaluation of relative robustness.

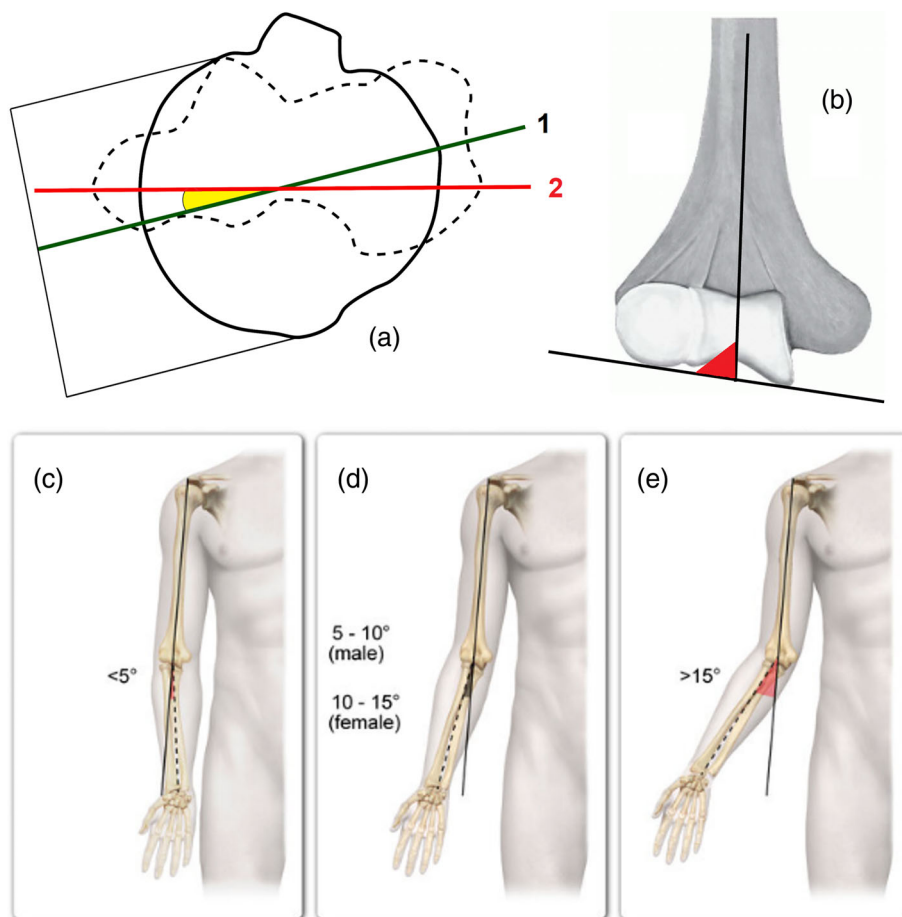
Additionally, although it may seem otherwise due to their greater cortical thicknesses, the overall strength of the humeral sections expressed by their section modulus “J” shows that the three complete SH humeri possess the overall strength to be expected when compared to present-day humeri of the same length (Rodríguez, 2013).

### 3.3.5 | Humeral retroversion angle

Humeral torsion refers to the orientation of the humeral head relative to the mediolateral axis of the distal humerus (twisting of one end of the humerus in relation to the other). However, there is a discord between the evolutionary and clinical definitions of this trait that contribute to the confusion concerning how to measure humeral torsion (Larson, 2007a, 2015; Rhodes, 2007). Furthermore, there are also some differences in the way to define the proximal humeral axis: a line bisecting articular margins of the humeral head at the anatomical neck, following Martin and Saller (1928) or Roach et al. (2012), drawn through the center of the humeral head dividing it into anterior and posterior halves (Rhodes & Churchill, 2009), or passing through the center of the head and the center point on the greater tubercle of the humerus (Patil et al., 2016).

Regarding this issue, here we prefer to follow the clinical presumption that the default condition for the hominin shoulder joint is to have a glenoid facing directly laterally and a humeral head pointing directly medially while the distal transversal axis is also mediolaterally oriented, that is, both axes, proximal and distal, are parallel or forming a zero-degree angle (Figure 7a). Deviation of the humeral head from this default to a more posterior orientation is called retroversion in the literature (Larson, 2007a, 2015). Retroversion is the angular complement to humeral torsion as traditionally measured, so increasing retroversion means reduced torsion and vice versa (see figure 1 in Larson, 2007a).

**FIGURE 7** (a) Retroversion angle of the humeral head as measured in this work. The outline of the proximal end is shown in proximal view with its mediolateral axis (green line, 1). The distal end is shown as a dashed line and the red line (2) is its transverse axis. (b) Cubital angle defined by Martin and Saller (1928) as variable M16. This angle is referred to in some medical literature as a Baumann's angle or sometimes as the carrying angle. The images below illustrate the most common representation of the carrying angle defined as the angle between the axis of the upper arm, usually the axis of humerus, and the axis of the forearm, usually the axis of the ulna. (c) In the cubitus varus deviation the carrying angle is very low,  $<5^\circ$ ; (d) represents the normal variation of the carrying angle in males and females; (e) in the cubitus valgus deviation the carrying angle is high, above  $15^\circ$ . Images c, d, and e from <http://www.coteillustration.com> (©UWorld)



As would be expected, recent humans display a wide range of retroversion angles averaging around  $25^\circ$ – $30^\circ$  (e.g., Edelson, 1999; Johnson et al., 2013; Kronberg et al., 1990; Larson, 2015). Martin and Saller (1928) report a range between  $45.5^\circ$  and  $16.0^\circ$  for 29 recent sample means and for example, Themido (1926) reports for a Portuguese sample of known sex, a mean of  $27.7 \pm 9.8$  for males ( $n = 42$ ), and  $22.6 \pm 9.5$  for females ( $n = 62$ ).

The retroversion angles of the three complete SH humeri (Table 4) as well as their average ( $40.7 \pm 6.4^\circ$ ) are toward the highest values reported for recent samples, as is also the case in the Neandertals (Carretero et al., 1997; Delsaux, 1977; Rodríguez, 2013; Rosas et al., 2006, 2015; Vandermeersch & Trinkaus, 1995). Our mean of the five Neandertal specimens where retroversion can be measured is  $35^\circ \pm 7.8$  (Lezetxiki =  $36^\circ$ ; La Ferrassie 1 =  $48^\circ$ ; La Chapelle Aux Saints =  $28^\circ$ ; Düseldorf =  $31^\circ$ ; Tabun C1 =  $32^\circ$ ). This means that the humeral head in the SH hominins, as well as in Neandertals, is more posteriorly facing than is the rule in recent humans, or that their torsion angle is lower.

Humeral torsion is an important variable that influences orientation and ranges of movement of the upper limb relative to the trunk (Kapandji, 1996). Some studies

indicate that the shape of the trunk of archaic hominins influences humeral torsion angle more than muscle activity (Churchill, 1996; Churchill & Rhodes, 2009; Cowgill, 2007; Rhodes & Churchill, 2009; Vandermeersch & Trinkaus, 1995). The anteroposterior expansion of the chest may influence the position of the scapula, which may be moved from a more coronal/lateral to a more parasagittal/anterior position. Reorientation of the glenoid fossa would necessarily lead to increased head retroversion to keep the elbow in the coronal plane. In this view, the relatively long clavicles of the Neandertals were also products of large chest size, needed to bridge the longer distance from the sternum to the acromion (Bastir et al., 2013; Churchill, 1996; García Martínez et al., 2014, 2020; Vandermeersch & Trinkaus, 1995).

On the other hand, some studies in the field of sports medicine indicate that individuals who engage in habitual throwing have increased humeral retroversion angles in their throwing arms and a greater degree of bilateral asymmetry in retroversion angles than nonthrowers (Kuhn, 2016; Larson, 2007b; Roach et al., 2012, 2013; Roach & Lieberman, 2014; Roach & Richmond, 2015). This view proposes that greater external rotational range of motion at the shoulder increases throwing velocity and

relates the high degrees of humeral retroversion in the fossil specimens to this activity. From this point of view, the scapular position of Neandertals would be more posterior in the thorax and the glenoid cavity more lateral, and in this case, clavicular elongation was most directly related to dorsal repositioning of the scapula (Larson, 2007a, 2007b, 2009). As we can see, determining the scapular position (more posterior or more lateral) and the relative clavicular length in fossil specimens is a key issue not easy to resolve (Melillo et al., 2019; Voisin, 2006) and which we have discussed in García-González et al. (2024).

Since the very beginning of our work on the SH fossils (Carretero et al., 1997), we have contended that the high humeral retroversion angle of the SH hominins is more related to their barrel-shaped thorax and broader general body form (Arsuaga et al., 1999, 2015; Bonmatí et al., 2010; Carretero et al., 2004, 2012), as is also the case for the adult and subadult Neandertals (Bastir et al., 2013; García Martínez et al., 2014, 2020; Gómez-Olivencia et al., 2009, 2018; Rosas et al., 2015; Vandermeersch & Trinkaus, 1995) than to habitual throwing. Nevertheless, we are aware that testing all these hypotheses requires additional fossil records and data on anatomical changes in the upper body that affect the ability to throw with power and accuracy (Roach et al., 2012). Regardless of the causes, it appears that a greater degree of retroversion indicates a greater ability to generate greater force in pulling motions because it increases the range of external rotation as the deltoid is more anteriorly positioned (Cowgill, 2007 and see below).

From a phylogenetical point of view, the retroversion angle is high not only in SH and the Neandertals, but in *Homo ergaster* KNM-ER WT-15000 (Walker & Leakey, 1993), *Homo georgicus* (Lordkipanidze et al., 2007), *Homo floresiensis* (Larson, 2007b, 2009; Larson et al., 2007), *Homo naledi* (Feuerriegel et al., 2017), *Australopithecus afarensis* (Alemseged et al., 2006; Stern Jr & Susman, 1983) and *Australopithecus sediba* (Churchill et al., 2013). This evidence would provide support for the plesiomorphic condition of a high retroversion angle within the hominins and the hypothesis of long-term continuity of this trait within the genus *Homo*. As all hominins show a high retroversion values, the lower degree of retroversion of recent humans would be a more recently derived condition. To note here that extant African apes are also characterized by a low degree of humeral retroversion and thus, the shared condition by recent humans and African apes seems to be a functional convergence (Larson, 2015) and a secondarily derived condition of *H. sapiens* within the hominins.

On the other hand, Krahl (1976) has demonstrated that humeral retroversion includes an ontogenetic

component in addition to a phylogenetic component in humans, which increases from birth until the proximal epiphyseal cartilage of the humerus disappears and bony fusion occurs. Moreover, Krahl (1976) noted that humeral rotator muscles provide the forces involved in the production of humeral torsion. Thus, the ontogenetic changes in humeral retroversion in subadult individuals seem to be an important issue. In this sense, we must remember the high degree of retroversion present in the subadults KNM-WT 15000 (Walker & Leakey, 1993) and Dmanisi individuals (Lordkipanidze et al., 2007), although, in the latter, it seems not to be lateralized.

In recent humans, humeral retroversion also decreases with age, with the highest values attained between birth and 2 years (Cowgill, 2007). The retroversion angle of the two SH complete subadult humeri is 59.6° in the younger H-XVII and 35° in the older H-IV. Thus, it seems that the same ontogenetic pattern is present also in the SH archaic hominins. The retroversion angle for H-XVII is toward the highest values for the equivalent age groups reported by Cowgill (2007: a mean retroversion angle for the age group between 6 and 9.9 years of 36.2° with a range between 9° and 66°).

Moreover, the retroversion angle of the older H-IV is close to the mean of its respective age group and also close to the retroversion angles showed by the adult specimens H-II and H-XV. For recent humans, the age group between 10 and 13.9 years old shows a mean retroversion angle of 34.4°, with a range between 12° and 62° (Cowgill, 2007). In recent humans, ontogenetic changes in the humeral retroversion angle cease between 16 and 20 years (Edelson, 1999; Krahl, 1976). The upper limit of the estimated age of the H-IV is 16 years old, thus, it is possible that this specimen had already attained its adult value, and considering this option, the retroversion angle for H-IV is toward the upper limit of recent hominin variation. This evidence seems to indicate that, as in adults, high retroversion angles also characterized subadult humeri from SH. In sum, the high humeral retroversion of SH adults and subadults, provides support for the hypothesis that this trait is highly related to general body form and that might be interpreted as part of a plesiomorphic configuration of the upper body of archaic hominins.

### 3.3.6 | Muscular impressions

As is the case in other bones, among the SH humeri, there is a large amount of variation in the humeral shaft muscular impressions, from very strong to weak. This variation is the same that can be observed in recent human humeri. Nevertheless, it is also true that the

majority of SH specimens have well-developed shaft insertions for the *Latissimus dorsi*, *Pectoralis major*, and *Teres major* muscles, as well as a broad bicipital groove (tendon of the *Biceps brachii*) and overall, a massive and well anteriorly projected lesser tubercle (insertion of the *Subscapularis*). This set of traits is good evidence of a strong shoulder musculature in most individuals. For some authors, the extraordinary development of the muscular impressions of the Neandertal humeral shaft set them apart from the pattern of recent humans (Thoma, 1975; Trinkaus, 1983; Trinkaus et al., 1994; Vandermeersch, 1991; Vandermeersch & Trinkaus, 1995). However, neither the muscular impressions nor robustness are necessarily linked to muscle development alone, and shaft dimensions and cross-sectional geometry also play an important role (see above). Additionally, we have calculated (Carretero et al., 2018) that the SH humeri and femora have around 25–35% more bone volume than recent bones of the same size, a trait that we relate with a heavier skeleton and much more muscular mass and body mass in these archaic hominins.

Regarding the deltoid tuberosity (DT) itself, in all the SH humeri, the aspect of this insertion is different from recent hominin morphology. The fossils show what we called “a close” or narrow DT (Carretero et al., 1997). The *Deltoid muscle* is divided into three parts (clavicular, acromial, and spinal deltoid) that have their reflection in three segments of the deltoid tuberosity (Gómez et al., 2020; Leijnse et al., 2008; Figure 8). The clavicular portion inserts in the anterior/ventral segment of the DT (on the anterior humeral border), the spinal portion inserts in the upper 2/3 of the lateral/dorsal segment of the DT while the acromial portion inserts in the distal 1/3 of the same segment (called the middle segment of the DT; Gómez et al., 2020).

When the SH humeri are observed in lateral view, it is very clear that the lateral/dorsal crest of the DT is rather vertical and less inclined backwards, or more centered in the lateral humeral surface, and does not reach the lateral border of the diaphysis (Figure 9). Thus, the form of the deltoid tuberosity of the SH humeri ( $n = 6$ ) is both, very consistent and distinctive, and different from the condition found in recent humans. Among the seven SH subadult humeri where it can be observed, the deltoid tuberosity displays the same morphological pattern as in adults.

Neandertals also have a “narrow” deltoid tuberosity (Carretero et al., 1997; Churchill, 1996; Endo, 1971; Endo & Kimura, 1970; Hublin et al., 1987; Rosas et al., 2006, 2015; Thoma, 1975; Vandermeersch, 1991; Vandermeersch & Trinkaus, 1995) and this is also the condition found in the scarce evidence for this anatomical region in early members of our genus (Carretero

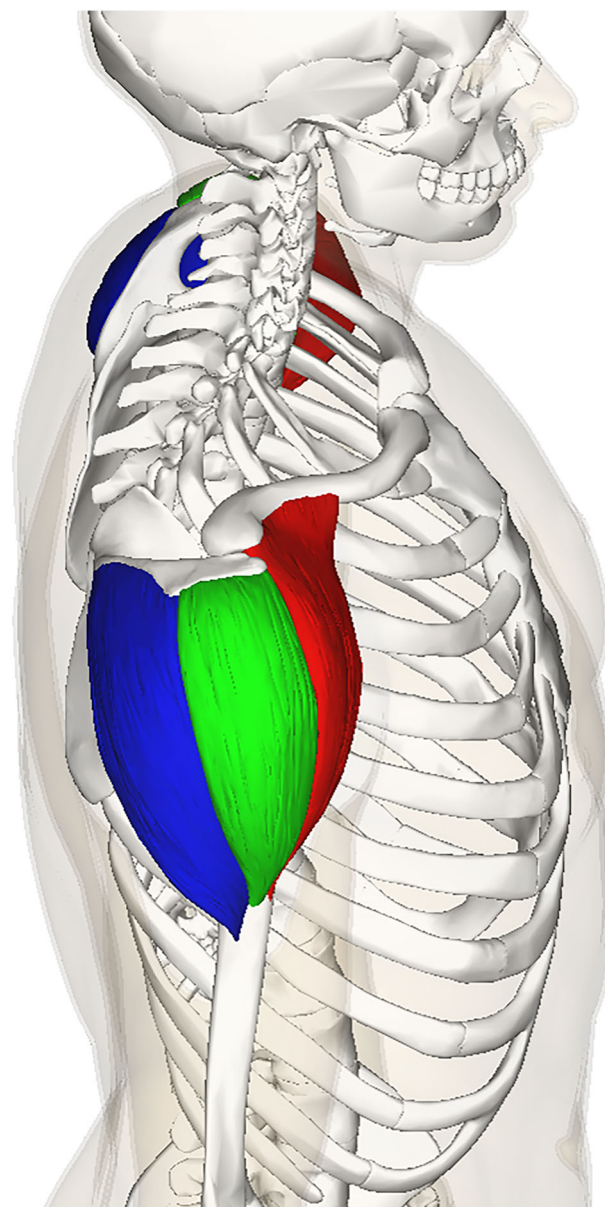


**FIGURE 8** The posterior/spinal (blue), lateral/acromial (green), and anterior/clavicular (red) portions of the deltoid muscle. From Anatomography BodyParts3D, Copyright 2008 Life Science Integrated Database Center licensed by CC Display-Inheritance 2.1 Japan, in Wikimedia commons, a free content repository hosted by the Wikimedia Foundation

et al., 1997: *Homo habilis* OH-62, *Homo ergaster* KNM-WT 15000 and *Homo erectus* from Zhoukoudian) as well as in the *A. afarensis* humerus AL-288-1m (Lovejoy et al., 1982). Thus, a narrow deltoid tuberosity shape seems to be the primitive condition for hominins.

The functional implication of this deltoid configuration is not fully clear at present, but as described above, the most conspicuous difference between the SH and recent humeri is the position of the insertion of the spinal portion of the *m. deltoideus* (the lateral crest). The

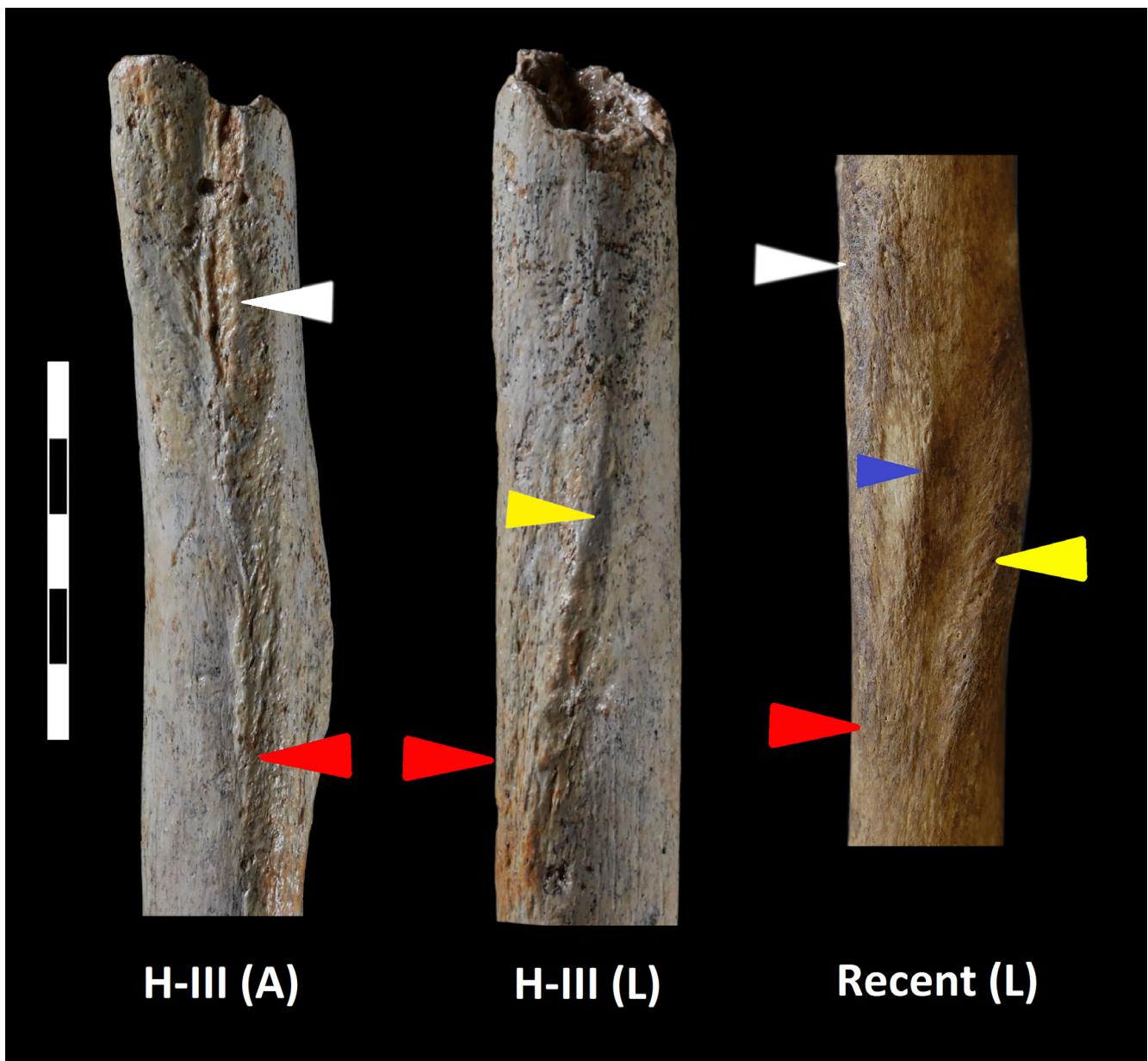


**FIGURE 9** Deltoid muscular crests in H-III from SH and a recent humerus. On the left and the middle H-III in anterior (A) and lateral (L) view, respectively. On the right, a modern human humerus from the collections housed at the University of Burgos. The white arrow points to the Pectoral Major insertion, the red arrow to the anterior deltoid crest, and the yellow arrow to the lateral deltoid crest. Note the commonly more open *H. sapiens* configuration with three clear muscular crests (red, yellow, and blue arrows) instead of the two almost constantly present in the fossil specimens. Scale in cm

primary function of the deltoid muscle in humans is the elevation of the forelimb in the scapular plane, with the clavicular (anterior) portion acting as a flexor and internal rotator of the glenohumeral joint, the acromial (central) portion as an abductor, and the spinal (posterior) portion acting as an extensor and external rotator. As mentioned above, it appears that a high retroversion angle indicates a greater rate of pull because it increases the range of external rotation as the deltoid is more “anteriorly positioned” (Cowgill, 2007). Thus, as is the

case in Neandertals (Churchill, 1996), the high retroversion and the peculiar morphology of the DT in the SH humeri (and other hominins) are associated (Carretero et al., 1997). Even if the shape of the DT is not directly caused by the high humeral retroversion, these two traits appear to be closely associated: high retroversion occurs with a more anteriorly positioned DT and more anteriorly displaced lateral crest (insertion of the spinal/posterior portion of the muscle). Nevertheless, it is not only the posterior deltoid that externally rotates the

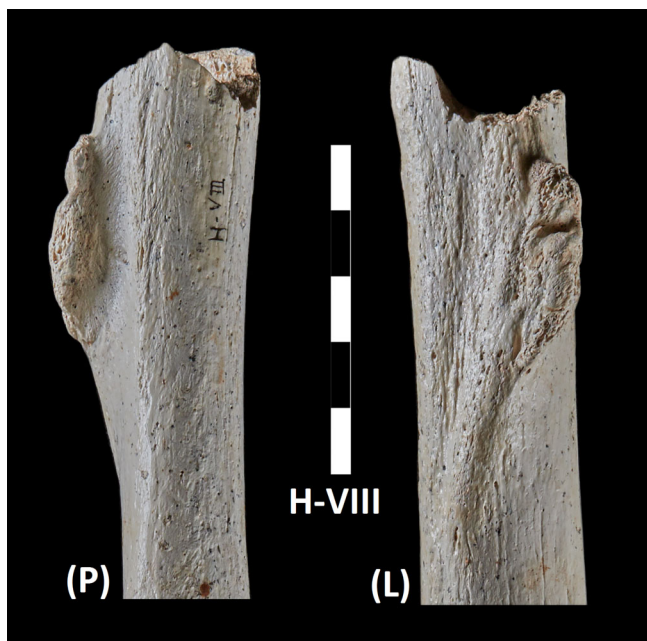


**FIGURE 10** Enthesopathy alteration on the lateral crest of the deltoid tuberosity of the left H-VIII from SH in posterior (P) and lateral (L) views whose etiology is compatible with a *myositis ossificans traumatica*. Scale in cm

glenohumeral joint, but the *m. infraspinatus* and *m. teres minor* are also very important. Thus, as is well known, the whole bony and muscular complex should be considered to functionally interpret any articulation. In this regard, we must keep in mind that the high retroversion angle that characterizes the fossil humeri apparently rotates the complete proximal epiphysis posteriorly, thus, while humeral head moves posteriorly, the greater and lesser tubercles and the bicipital sulcus moves anteriorly, and with them, the insertions of rotator cuff muscles and *m. biceps brachii*. This scrolling seems to be favorable for the dorsal muscles, but apparently not so much for the subscapular and other ventral muscles with insertions on the proximal-anterior region of the humeral shaft.

Finally, we note here too that the right H-VIII, one of the largest specimens, shows a massive and conspicuous enthesopathy alteration on the lateral crest of the deltoid tuberosity (Figure 10). The etiology of this alteration is under study but its macroscopical image fits with a *myositis ossificans traumatica*, a condition where bone tissue forms inside muscle or other soft tissue after an injury. It tends to develop in young adults and athletes who are more likely to experience traumatic injuries and most of the time occurs in the large muscles of the arms or the legs (see e.g., Beiner & Jokl, 2002; Cushner & Morwessel, 1992).

The debate about to what extent these humeral (and other shoulder girdle traits, see García-González et al.,

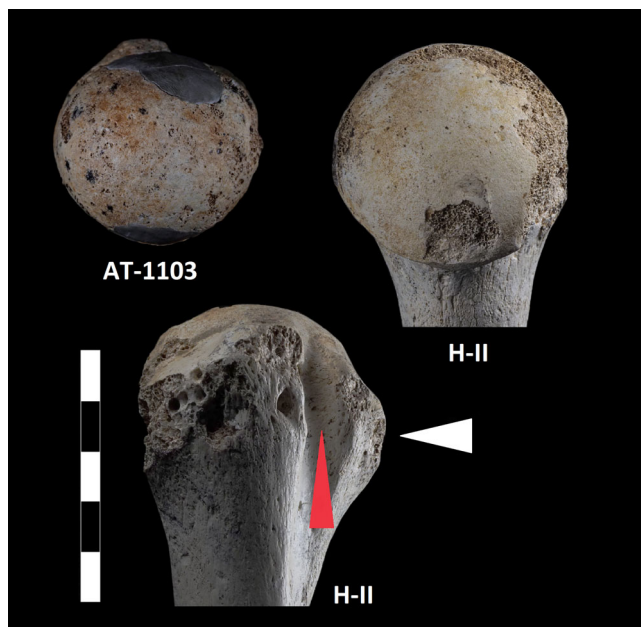


**FIGURE 11** Above: proximo-medial view of the humeral heads AT-1103 and H-II as examples of its transversely oval shape. Below: proximal epiphysis of the H-II in lateral view showing the massive lesser tubercle (white arrow) and the broad bicipital sulcus (red arrow). Scale in cm

2024) of SH and Neandertals are related to a particular body shape configuration, to a particular behavior and arm use, or both, is still open. The kinds of behavior/s or physical activities that could generate frequent and large external rotation to develop these arm adaptations are not clear cut, but habitual overhead high-speed throwing or frequent knapping and lithic tool use have been largely discussed (Churchill, 1996; Churchill & Rhodes, 2009; Larson, 2007b, 2009, 2015; Roach & Lieberman, 2014; Roach & Richmond, 2015). Obviously, some other activities come to our mind that could be introduced into the equation: stalking and close-range hunting (spearing), breaking bones, butchering, defleshing, and transporting meat, stones, prey, or any other materials. Additionally, Shaw et al. (2012) consider that scraping activities, such as hide preparation, may be a key behavior in determining the unusual pattern of Neandertal arm morphology.

### 3.3.7 | The proximal epiphysis

The five SH preserved proximal epiphyses where the head can be measured are characterized by a clearly transversely oval humeral head, that is, transverse or mediolateral diameter is greater than the vertical or sagittal one (Figure 11). This trait is constant regardless of the

side and size of the specimens and can be considered another upper limb feature linked to their different upper body shape (Arsuaga et al., 2015). A transversely oval humeral head also characterizes the Neandertals (Boule, 1911–1913; McCown & Keith, 1939; Basabe, 1966; Heim, 1982; Rosas et al., 2015), while the opposite condition, that is, a vertically oval humeral head, is the rule in recent humans (Carretero et al., 1997; Dittrick & Suchey, 1986; Krogman & Yasar-Iscan, 1986; Themido, 1926).

The humeral head is vertically oval in *Ardipithecus ramidus* from Aramis (Lovejoy et al., 2009; White et al., 1994), in *Au. afarensis* and *Au. africanus* specimens and in the taxonomically unaffiliated specimen KNM-ER 1473 from East Turkana (pers. observ., Lovejoy et al., 1982; Carretero et al., 1997) and is also vertically oval in *Au. sediba* (Churchill et al., 2013; Feuerriegel et al., 2017). Unfortunately, neither the Nariokotome partial skeleton KNM-WT 15000 nor *H. georgicus* (Lordkipanidze et al., 2007), *H. floresiensis* (Larson et al., 2009), or *H. naledi* (Feuerriegel et al., 2017) specimens preserve the humeral heads. Nevertheless, Feuerriegel et al. (2017) estimate humeral head diameters for the *H. naledi* U.W. 101-283 right humerus, indicating a vertically oval humeral head. Thus, the limited evidence points to a vertically oval humeral head as the primitive condition for the hominins and a transversely humeral head as a derived morphology for at least the European Neandertal lineage.

As is the case for the previously mentioned shaft traits, the specific functional meaning, if any, of the transversely oval humeral head is not clear, but is likely linked with the shaft traits described above and overall, with the scapular glenoid fossa morphology. In SH (Carretero, 1994; Carretero et al., 1997; García-González et al., 2024) and the Neandertals (Churchill & Trinkaus, 1990; Di Vincenzo et al., 2012; Trinkaus, 1983) this humeral head morphology is present along with a narrower glenoid cavity of the scapula. The most obvious effect of this morphology of the glenohumeral articulation is enhancing ranges of motion of external and internal rotation at the shoulder joint. Again, the rotator cuff and the posterior and anterior deltoids are likely implicated.

A relatively narrow scapular glenoid cavity suggests high levels of joint reaction forces at the articulation (Churchill & Trinkaus, 1990; Lieberman et al., 2001), and together with a broader humeral articular head could mean also less shoulder joint congruency or stability in the SH and Neandertals archaic hominins. As mentioned above, the glenohumeral joint congruency is maintained primarily by the rotator cuff muscles inserted into the articular capsula and, if the shoulder joint is

morphologically and mechanically “less stable” (more labile) then, muscular hypertrophy should help to maintain the articular stability. It is not clear whether the dorsoventral range of movement of this configuration is narrower than in recent humans, as a transversally expanded humeral head could compensate for the narrow glenoid cavity. Again, although these mechanical details must be still demonstrated, it is also reasonable to relate shoulder morphology with a necessary adjustment to the barrel-shaped thoraxes of both groups (SH and *H. neanderthalensis*).

The greater tubercle does not look especially robust in any SH specimen but, whatever the development of the shaft muscular impressions, all of them show a massive (inflated) and anteriorly well-projecting lesser tubercle, a condition that can be found also in Neandertals (Basabe, 1966; Carretero et al., 1997; Rosas et al., 2015; Vandermeersch & Trinkaus, 1995). This massive lesser tubercle can be related to a strong *m. subscapularis*, an important part of the rotator cuff that stabilizes the shoulder joint anteriorly. Fossil record of the early hominin proximal humerus is extraordinarily scant and fragmentary (Sts 7, KNM-ER 1473, KNM-BC 1945, Omo 119-73-2718, A.L. 288-1r, A.L. 333-107 and A.L. 333-87) but the lesser tubercle is described as very elongated and often protruding (Senut, 1981). Carretero et al. (1997) considered unclear the phylogenetic significance of the massive lesser tubercle shared by SH hominins and the Neandertals, but Larson (2007b) comments that an enlarged lesser tubercle in the SH and Neandertals is reminiscent of the condition in these early hominins proximal humeri and that, in this case, it may represent a retention of the primitive condition for hominins. Although reasonable, the lack of fossil evidence for the *Homo* lower Pleistocene hominines, makes for the moment a clear phylogenetic interpretation difficult. Finally, the bicipital groove is broad and deep, overall, at midway between the two tuberosities, reflecting probably a powerful tendon for the long head of the *m. biceps* (Figure 11). It should be noted finally, that a transversely oval humeral head with a massive lesser tubercle also characterizes the proximal epiphysis of subadult individuals from SH (Figure 1) which demonstrates that these morphologies are already present at early stages in ontogeny and suggests they are mainly genetically controlled.

### 3.3.8 | Distal medial and lateral epicondyles

All SH specimens display a well-developed lateral epicondyle, projecting and set high with respect to the capitulum, but not outside the normal recent human range of variation. This is also the case in Neandertals (Rosas

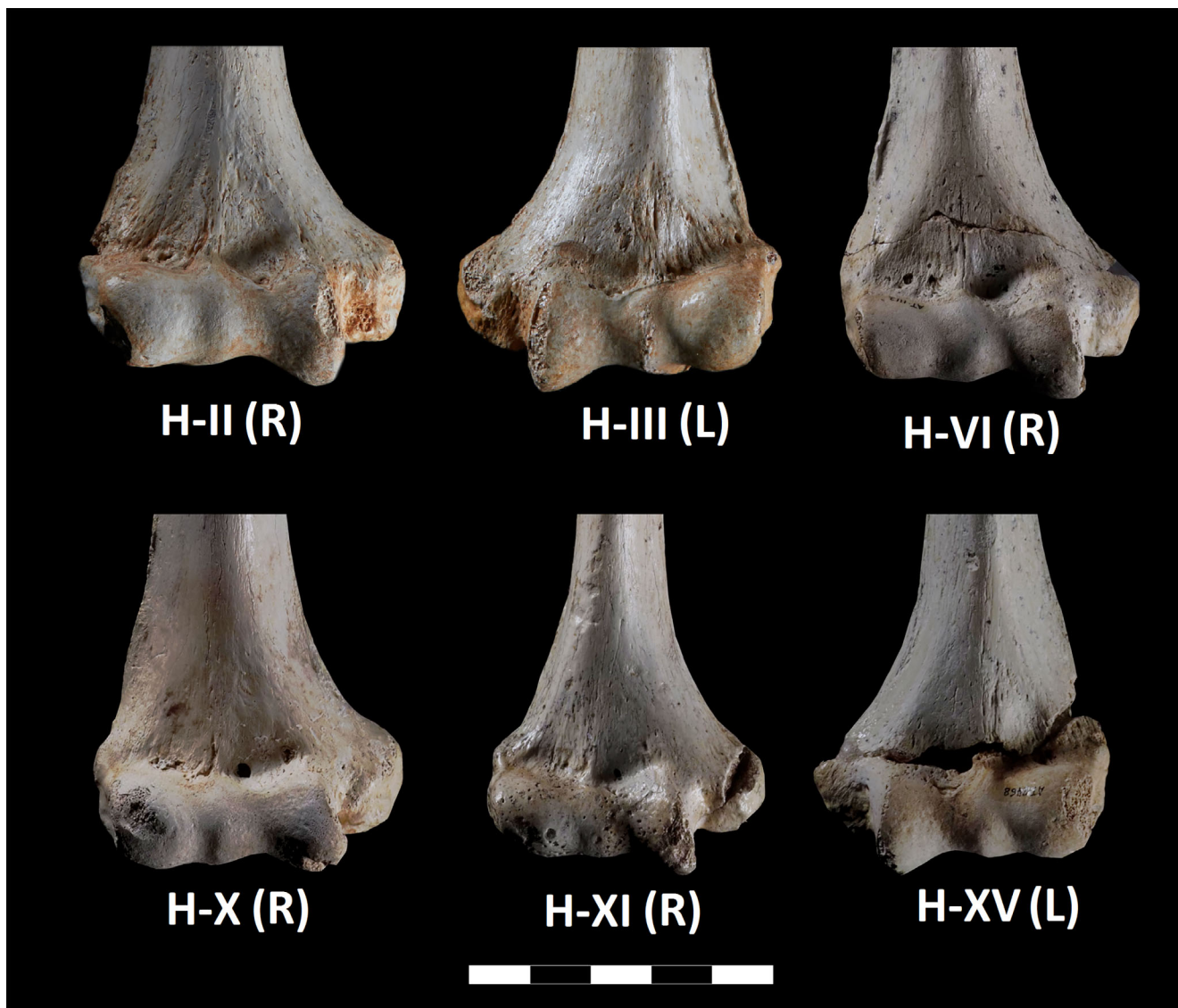


FIGURE 12 Anterior view of six distal epiphyses of SH humeri. R, right humerus; L, left humerus. Scale in cm

et al., 2015). On the contrary, a greater medial projection, thickness, and posterior deviation is a conspicuous condition of the medial epicondyle in Neandertals (Heim, 1982; McCown & Keith, 1939; Senut, 1981; Smith, 1976; Trinkaus, 1983; Vandermeersch, 1991; Vandermeersch & Trinkaus, 1995). According to Galtés et al. (2008) the greater projection of the medial epicondyle favors forearm pronation as it maximizes the distance between the insertion of the *m. pronator teres* on the radius and on the humerus. Although the medial epicondyle is very robust, very thick, and well-medially projected in the SH humeri, it is somewhat more variable regarding its posterior deviation (Figures 12 and 13). The SH range of variation for the medial epicondyle angle ( $13^{\circ}$ – $21.5^{\circ}$ ,  $n = 5$ ; Rodríguez, 2013) is virtually identical to the range reported by Vandermeersch and Trinkaus (1995) for the Krapina Neandertal sample ( $14$ – $22^{\circ}$ ,

$n = 7$ ). Both fossil samples fall within the upper half of the recent human range of variation reported by these same authors ( $5$ – $25^{\circ}$ ;  $n = 50$ ). Thus, despite the large variation, the SH hominins and Neandertals tend to show a marked posterior deviation of the medial epicondyle more frequently than modern humeri.

### 3.3.9 | Shape of the distal articular surface

The trochlea of SH humeri is characterized by blunt and less projected medial and lateral borders and a shallow trochlear groove compared with recent humeri. Probably related to this, the capitular shape in the SH sample is also different from recent modern humeri. First, the capitulum is less anteriorly projected relative to the medial or lateral lips of the trochlea and is less medially

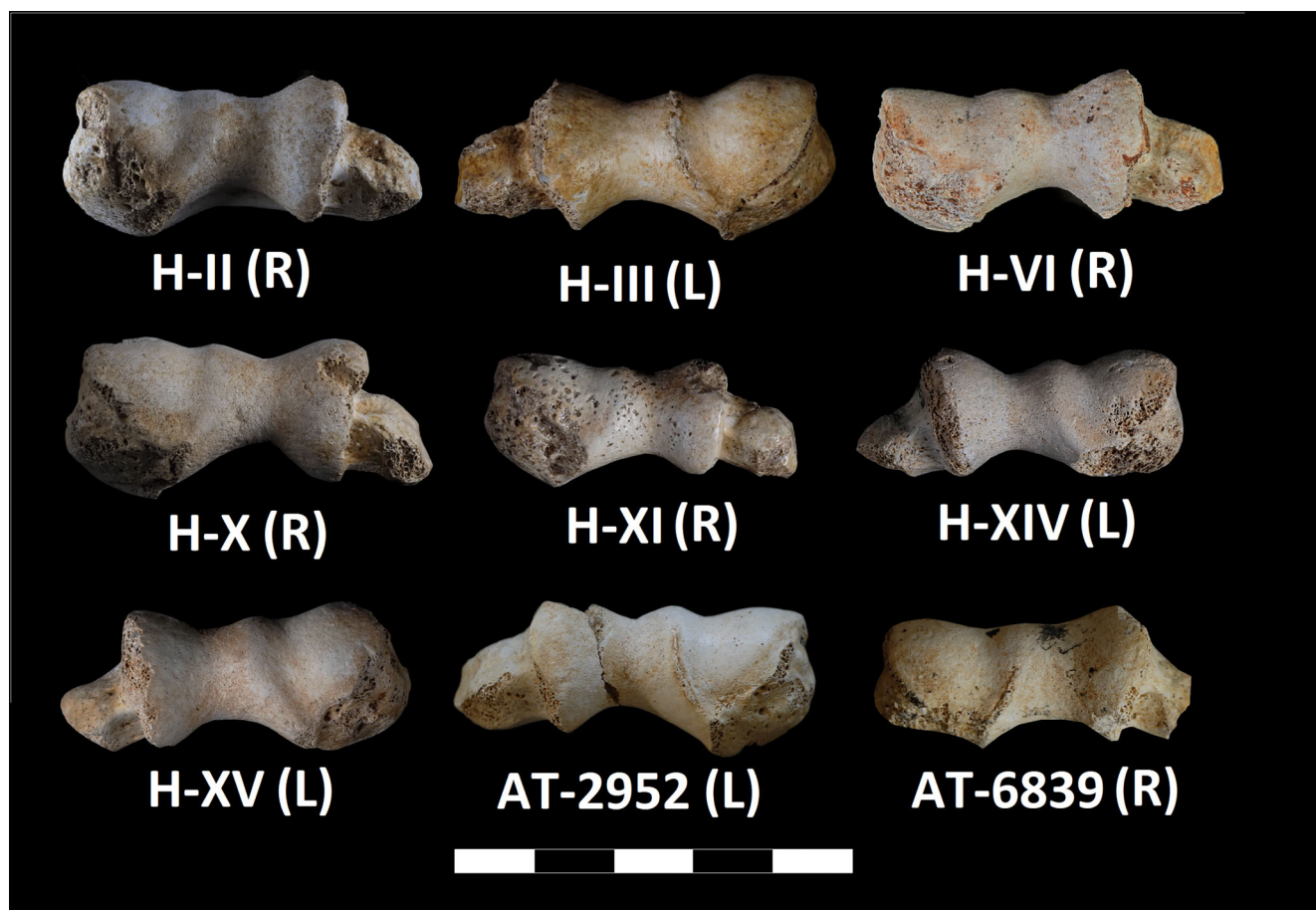


FIGURE 13 Inferior view of nine distal epiphyses of SH humeri. Anterior is up. R, right humerus; L, left humerus. Scale in cm

rotated (oriented). Second, most specimens have a relatively broad capitulum, only slightly higher than broad or even somewhat expanded mediolaterally as indicated by its high capitular index, usually above 90% (Table 4; Figures 12 and 13). This is also the condition more common in Neandertals. In contrast, the most common morphology found in recent humeri is a relatively narrow capitulum. Using a simple index of breadth on height, we have not found significant differences between the SH, Neandertal, and some recent sample means (Carretero et al., 1997; Rodríguez, 2013) and the trait is in fact quite variable in all samples. Nevertheless, on average, the SH specimens show the same tendency as the Neandertals toward a relatively broad capitulum (higher capitular index) (SH average =  $93.2 \pm 4.8$ ,  $n = 7$ ; Neandertal average =  $97.6 \pm 10$ ,  $n = 19$ ; recent medieval sample =  $83.4 \pm 6$ ,  $n = 30$ ).

In the subadult specimens, H-IV and the isolated distal end AT-1117, the capitulum can be measured with confidence and both specimens display the same tendency as the adults toward a relatively broad morphology (capitulum shape index of 90.5 and 92.5, respectively). Nevertheless, the subadult status of these epiphyses advises us to take this information with caution (Figure 2).

### 3.3.10 | Cubital and carrying angles

As expected by the shallow trochlear shape, on average the SH adult maximum cubital angle ( $85.4 \pm 2.1$ ,  $n = 5$ ; Figure 7b) is also high and at the upper limit of the range of variation reported by Martin and Saller (1928) for seven recent human sample means (77.0–84.5). This is also the case for the Neandertals ( $84.2 \pm 2.1$ ,  $n = 12$ ; Trinkaus, 1983; Vandermeersch & Trinkaus, 1995). The cubital angle is, at least in part, the expression of the *carrying angle* when we only have at hand the humerus. The carrying angle is formed by the axis of the humerus with that of the ulna (Figure 7c–e). Normally, the forearm is aligned in valgus with respect to the arm in full extension, with medial angulation called the carrying angle that ranges between  $5^\circ$  and  $20^\circ$  as the normal condition in recent humans (An et al., 1983; Beals, 1976; Paraskevas et al., 2004; Figure 7d). Since the carrying angle is in part due to the more distal position of the tip of the medial lip of the trochlea and thus, to the cubital angle, and both are negatively related, a higher cubital angle suggests less valgus deviation of the forearm. Thus, although within the normal range, the SH hominins and

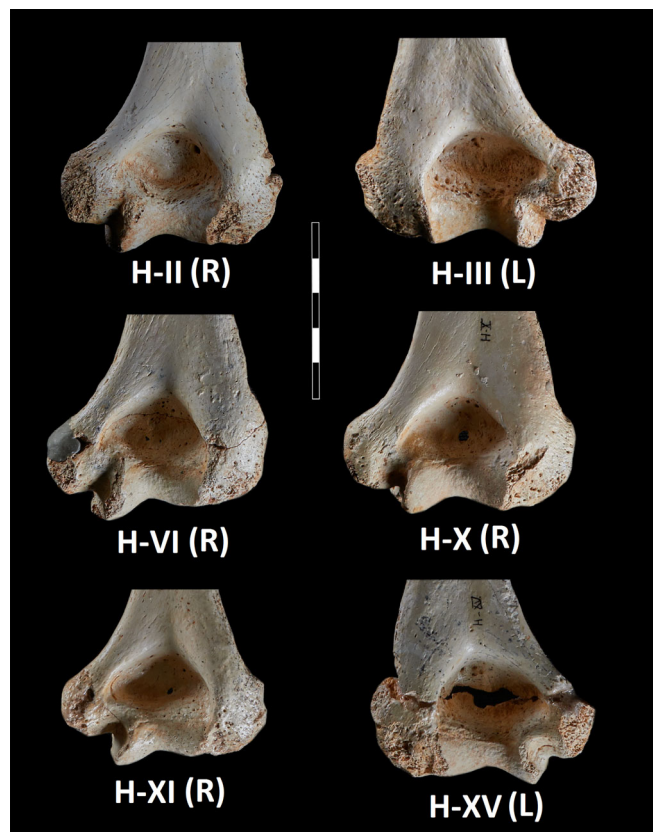


**FIGURE 14** Posterior view of same six distal epiphyses of Figure 12. R, right humerus; L, left humerus. Scale in cm

the Neandertals are at the lower limit of the normal valgus deviation of the forearm.

The significance of the carrying angle is not yet fully defined, and although it is important when carrying objects, it varies with sex, age, handedness, forearm muscular strength, ulna and radius length, stature, body constitution, and even hip width and hormonal factors (An et al., 1983; Beals, 1976; Kumar et al., 2010; Paraskevas et al., 2004; Steel & Tomlinson, 1958). Thus, in the case of SH and the Neandertals, it could be also influenced by thorax shape, although to what extent is not yet determined. The carrying angle of the elbow tends to decrease with increasing humeral retroversion (Larson, 2015), therefore, this fits in with what was said above about the high retroversion angle of the SH specimens.

### 3.3.11 | Olecranon fossa and distal pillars

All adult distal epiphyses of SH humeri have large, wide, and deep olecranon fossae in absolute terms and when compared with the biepicondylar breadth. Related to this, the medial pillar surrounding the fossa is thinner relative to biepicondylar breadth than in recent hominin humeri (Arsuaga et al., 2015; Carretero et al., 1997;



**FIGURE 15** Standard anatomical views of the H-II. A, anterior; L, lateral; P, posterior; M, medial. Scale in cm



**FIGURE 16** Standard anatomical views of the H-III. A, anterior; L, lateral; P, posterior; M, medial. Scale in cm

Rodríguez, 2013; Figure 14). Among the subadult specimens, H-XII shows an absolutely and relatively wide olecranon fossa compared with the 9–11 years age group of modern children. However, this is not so clear for H-



**FIGURE 17** Standard anatomical views of the H-VI. A, anterior; L, lateral; P, posterior; M, medial. Scale in cm

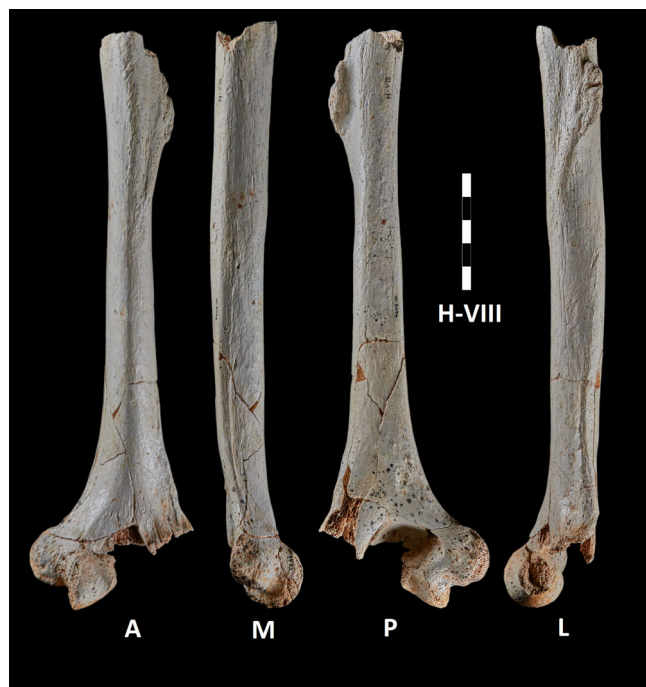


**FIGURE 19** Standard anatomical views of the H-VIII. A, anterior; L, lateral; P, posterior; M, medial. Scale in cm



**FIGURE 18** Standard anatomical views of the H-VII. A, anterior; L, lateral; P, posterior; M, medial. Scales in cm

IV (Table 7). In this specimen, olecranon fossa breadth falls well within the normal range of variation of the 12–16 year age group of modern humeri, either with fused or unfused distal epiphyses (Table 7). Both H-IV and H-XII show a medial pillar that is relatively and absolutely



**FIGURE 20** Standard anatomical views of the H-X. A, anterior; L, lateral; P, posterior; M, medial. Scale in cm

thinner than their respective recent hominin age groups, as is the case for the adult humeri (Figures 3–6).

Within the European fossil record, we have described this set of distal humeral features in the adult and



FIGURE 21 Standard anatomical views of the HX-I. A, anterior; L, lateral; P, posterior; M, medial. Scale in cm

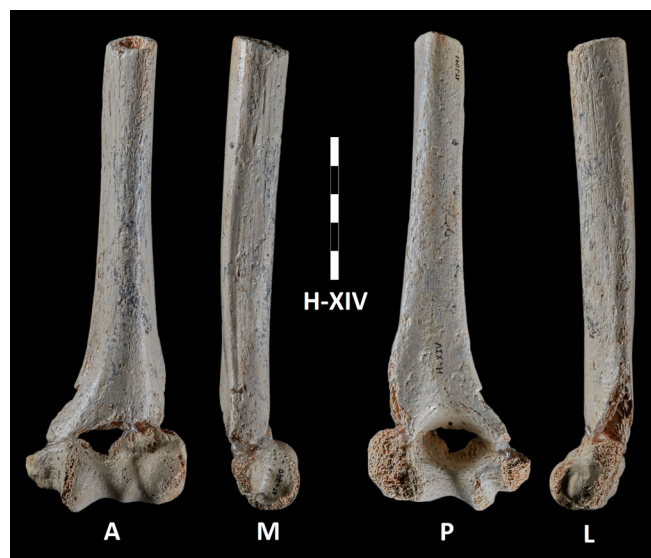


FIGURE 22 Standard anatomical views of the H-XIV. A, anterior; L, lateral; P, posterior; M, medial. Scale in cm

subadult Early Pleistocene specimens of *Homo antecessor* from Gran Dolina (Bermúdez de Castro et al., 2012). Thus, this set of elbow traits is present in Europe in the Early (*H. antecessor*), Middle (SH), and Late (Neandertals) Pleistocene hominins. On the contrary, a relatively small and narrow olecranon fossa and thick medial and lateral adjacent pillars are the most frequent condition in recent and early *H. sapiens* (Carretero et al., 1997), although some variation is found in Upper



FIGURE 23 Standard anatomical views of the H-XV. A, anterior; L, lateral; P, posterior; M, medial. Scale in cm



FIGURE 24 Anterior view of other incomplete adult humeral specimens from Sima de los Huesos. R, right humerus; L, left humerus. Scale in cm

Paleolithic and recent samples (Carretero et al., 2009; Shang et al., 2007; Shang & Trinkaus, 2010), reflecting the natural frequency of this trait in our species. The

TABLE 8 State of some morphological features of the humerus in different hominins.

Trait	Australopith. <sup>a</sup>	Other Pleistocene <i>Homo</i> species <sup>b</sup>	SH adults <sup>c</sup>	SH subadults	Neandertals Adults/subadults	Modern <i>Homo sapiens</i>
Shape of the humeral head	Vertically oval	Vertically oval	Transversely oval	Transversely oval	Transversely oval	Vertically oval
Lesser tubercle	Projecting and massive?		Projecting and massive	Projecting and massive	Projecting and massive	Narrower and flatter
Intertubercular sulcus	Shallow rather than deep		Wider and deeper	Wider and deeper	Wider and deeper	Narrower and shallower
Absolute humeral length			Variable		Variable	Variable
Diaphyseal shape			Variable	Variable	Variable	Variable
Shaft robusticity	Variable		Variable		Variable	Variable
Torsion angle	Low	Low	Low	Low	Low/low	Higher
Retroversion angle	High	High	High	High	High/high	Lower
Deltoid tuberosity	Narrow with two crests	Narrow with two crests	Narrow with two crests	Narrow with two crests	Narrow with two crests	Wide with three crests
Cortical bone thickness <sup>d</sup>			Thick		Thick	Thinner
Shaft muscular entheses			Variable	Variable	Stronger	
Distal articular size relative to biepicondylar breadth			Large	Variable	Large/variable	Smaller
Medial epicondyle			Robust and more posteriorly oriented		Robust and more posteriorly deviated	Smaller and more medially oriented
Olecranon fossa relative breadth and depth <sup>e</sup>	Narrower and shallower	Narrower and shallower	Wider and deeper	Wider and deeper	Wider and deeper	Narrower and shallower
Medial pillar relative thickness <sup>f</sup>	Thicker	Thicker	Thinner	Thinner	Thinner	Thicker
Capitulum shape	Taller than wide	Taller than wide	Wider than tall	Wider than tall	Wider than tall	Taller than wide
Cubital angle			High		High	Lower
Carrying angle			Low		Low	Higher
Trochlear medial sulcus	Deep	Deep	Shallow	Shallow	Shallow	Deep

<sup>a</sup>Specimens attributed to the genus *Ardipithecus*, *Australopithecus*, and *Paranthropus*.

<sup>b</sup>Specimens attributed to *H. habilis*, *H. ergaster*, *H. erectus*, *H. georgicus*, *H. naledi*, and *H. floresiensis*.

<sup>c</sup>Fossil record from the Non-SH Middle Pleistocene hominins is nonexistent for most humeral anatomical regions.

<sup>d</sup>Also thick in the lower Pleistocene *H. antecessor* ATD6-121 subadult and ATD6-148 adult specimens (Bermúdez de Castro et al., 2012) and in the African Middle Pleistocene specimen from Bodo (BOD-VP-1/2; Carretero et al., 2018).

<sup>e</sup>Olecranon fossa also wider and deeper in lower Pleistocene *H. antecessor* ATD6-121 subadult and ATD6-148 adult specimens (Bermúdez de Castro et al., 2012) and in the African Middle Pleistocene specimen from Bodo (BOD-VP-1/2; Carretero et al., 2018).

<sup>f</sup>Medial pillar is also thinner in lower Pleistocene *H. antecessor* ATD6-121 subadult and ATD6-148 adult specimens (Bermúdez de Castro et al., 2012) and in the African Middle Pleistocene specimen from Bodo (BOD-VP-1/2; Carretero et al., 2018).

available australopithecine distal humeri ( $n = 7$ ), show the recent human condition (Carretero et al., 1997; Churchill et al., 2013; Senut, 1981), while within Early and Middle Pleistocene *Homo* from Africa, some variation is also detected. While KNM-WT 15,000 and the

distal humeri from Gombore IB-7594 and Kabwe show the australopithecine and *H. sapiens* condition (Chavaillon et al., 1977; Di Vincenzo et al., 2015; Senut, 1981; Yokley & Churchill, 2006), the African Middle Pleistocene specimen from Bodo (Middle Awash,

Ethiopia) displays the European (SH and Neandertal) morphology (Carretero et al., 2009). More recently, the distal humeral morphology of *Homo naledi* (Feuerriegel et al., 2017) while absolutely smaller, appears to fit the same pattern of relatively thin pillars and wider olecranon fossae seen for Early, Middle, and Late Pleistocene European hominin samples and Bodo.

In sum, although the phylogenetic significance of this morphological pattern is still unclear, both olecranon fossa patterns are fairly consistent. More variation is found among African hominin fossils than among the European fossil record and recent samples, which suggests a possible basal polymorphism as we proposed in Carretero et al. (2009) and Bermúdez de Castro et al. (2012). A large and deep fossa with rather thin pillars adjacent to it is, up to now, constant among the European archaic hominins of the Early, Middle, and Upper Pleistocene and, accordingly, seems to be fixed among European archaic Pleistocene hominins since almost 1 million years. Thus, this morphology (or its high frequency) can be considered, at this time, as a characteristic of this/these European lineages.

### 3.3.12 | Distal articular relative size

Relative to maximum length, the SH adult humeri exhibit distal articular breadth and biepicondylar breadth proportions indistinguishable from those of recent humans, as is the case for the complete Neandertal humeri (Carretero et al., 1997). However, the relative proportion of distal articular breadth to biepicondylar breadth is on average larger in SH and the Neandertals than in many recent samples (Carretero et al., 1997; Rodríguez, 2013). Although not significant, these differences indicate a tendency in the SH fossils toward relatively larger humeral distal articular dimensions, as is the case in the Neandertals (Churchill & Trinkaus, 1990). Nevertheless, again variation is the rule within the SH sample. While H-II and III have articular proportions slightly above the Neandertal and recent means, H-XIV is more than 2 *SD* above the same averages, and H-VI and AT-1110 fall in between (SH average =  $74.0 \pm 1.7$ ,  $n = 7$ ; Neandertal average =  $73.0 \pm 2.6$ ,  $n = 15$ ; Recent Samples =  $72.5 \pm 3.0$ ,  $n = 154$ ; Carretero et al., 1997).

The relative distal metaphyseal breadth of the subadult specimens varies with age (Table 7). While the younger SH specimen (H-XII) shows a relatively large distal end, the older individual (H-IV) does not. An absolutely and relatively large humeral distal end does not characterize all subadult Neandertals either, although this trait seems to appear early in

development. For example, it is detected in Dederiyeh 1 at around 1.5 years old, but it is not present from birth since the neonatal individual of Le Moustier 2 does not show this trait (Bermúdez de Castro et al., 2012). Thus, the differences between the two SH specimens can be due to merely individual idiosyncrasy, although obviously other sources of variation cannot be discarded. We must consider, however, that sample size for such young Neandertal individuals are extremely small, and it is unclear how variable this feature may be between individuals and throughout ontogeny. For example, it may be that Le Moustier 2 is idiosyncratic in this case and does not reflect the most common state of this trait in Neandertal infants.

## 4 | CONCLUSIONS

The detailed postcranial anatomy of the genus *Homo* has changed in the last 2 million years, and some of these changes have postural and/or biomechanical implications. Thus, a combined understanding of the postcranial evolution at both a general and a more specific level are of high interest to paleoanthropologists. The Middle Pleistocene SH fossil collection provides the rare opportunity to thoroughly characterize the postcranial skeleton in a fossil population, only comparable to that obtained in the study of the Neandertal hypodigm and recent humans.

The SH humeri (Figures 1–5 and 12–24) display a consistent morphological pattern that distinguishes them from recent humans and brings them closer to the Neandertals. This pattern includes (Table 8):

### Diaphysis

- Highly variable humeral length, although on average are long compared with recent human samples and those of Neandertals.
- Variable diaphyseal shape and robusticity. This trait is also observed in subadults.
- Thicker cortical walls along the shaft like Neandertals. This trait is also observed in subadults. Primitive condition.
- Mechanical cross-sectional properties (Ix, Iy, and J) are not significantly different from recent medieval populations once the size is considered.
- Variable muscular impressions and entheses on the diaphyses.
- Narrow deltoid tuberosity with two muscular crests (like the Neandertals). This trait is also observed in subadults. Primitive condition.

## Proximal epiphysis

- Elevated retroversion angle (low torsion angle) of the proximal epiphysis on average (like the Neandertals). This trait is also observed in subadults. Primitive condition.
- Transversely oval humeral head (like the Neandertals). This trait is also observed in subadults. Derived condition of Neandertal lineage.
- Swollen, massive, and quite anteriorly projected lesser trochanter (like the Neandertals). This trait is also observed in subadults. Probably the primitive condition.
- Deep and broad bicapital sulcus.

## Distal epiphysis

- Variable distal articular size relative to biepicondylar breadth. In subadults, the relative distal metaphyseal breadth is variable with age.
- Thick, massive, and posteriorly curved medial epicondyle (like the Neandertals).
- Relatively broad and low capitulum (high frequency) (like the Neandertals). Derived condition of Neandertal lineage.
- Shallow trochlea with less projected medial and lateral rims (like the Neandertals). Derived condition of Neandertal lineage.
- Elevated cubital angle on average (or low carrying angle) that leads to a low valgus deviation of the fore arm relative to the upper arm (like the Neandertals).
- Broad and deep olecranon fossa (like the Neandertals). This trait is also observed in subadults. Derived condition of Neandertal lineage.
- Relatively narrow lateral and medial distal pillars surrounding the olecranon fossa (like the Neandertals). This trait is also observed in subadults. Derived condition of Neandertal lineage.

In short, the SH humeri share with the Neandertals many traits usually considered to be Neandertal specializations that certainly are not. This evidence is consistent with the hypothesis based on the cranial and postcranial morphology that the SH hominins are a sister group to the later Neandertals (Arsuaga et al., 2014, 2015). Some of the humeral shared traits seem to be primitive features within the genus *Homo* or even for all hominins, such as the low torsion angle, narrow deltoid tuberosity with two crests or the thick cortical walls. Others display high variability within different hominin samples and are of uncertain

phylogenetic value, such as the humeral length, the shape and robusticity of the diaphyses, the relative size of articular surfaces, and the muscular impressions. This variation found within the fossil and recent samples stress the natural frequency of most traits (Carretero et al., 1997, 2009). However, many of them are significantly more frequent in the SH hominids and the Neandertals, such as the relatively deep and broad olecranon fossa, the relative thin medial and lateral distal pillars, the transversely oval humeral head, the massive and very protruding lesser tubercle, the relatively broad and low capitulum and the elevated cubital angle. Thus, the high frequency of these traits characterizes both, SH and Neandertal samples, and might be considered as “exclusive” to this European phyletic lineage of *Homo*.

The cranial and dental evidence from SH suggests that the full suite of derived Neandertal features did not emerge as a single package, but that different features appeared separately and at different times, illustrating the process of mosaic evolution (Arsuaga et al., 2014) and supporting the accretion model of Neandertal origins (Hublin, 2009). Moreover, the pattern of morphological change shows that the Neandertal-derived regions of the SH skulls are functionally related to the masticatory complex, suggesting that the origin of the Neandertal clade coincides with a masticatory specialization (Arsuaga et al., 2014). The overall SH postcranial evidence is consistent with this hypothesis (Arsuaga et al., 2015), although the pattern of morphological change in functionally related modules is not yet well determined. In the specific case of the humerus, most of the phylogenetically relevant characteristics of the Neandertals were already present in their SH ancestors, except maybe the length variation and therefore, the upper limb proportions.

The shoulder girdle is a highly functional complex indeed related to the neck, shoulder, elbow, and wrist that shows a complicated evolutionary history in the hominin fossil record. The detailed discussion of the evolution and functional implications of the entire shoulder girdle in SH and other hominins is far beyond the scope of this paper, but the recovery and reconstruction of new specimens and associations to one and the same individual, from both, SH Middle Pleistocene and Gran Dolina TD-6 Early Pleistocene sites at the Sierra de Atapuerca, probably will allow future studies of the entire shoulder girdle complex with greater confidence.

## AUTHOR CONTRIBUTIONS

**José-Miguel Carretero:** Conceptualization; formal analysis; investigation; methodology; supervision; validation; writing – original draft; writing – review and editing.  
**Laura Rodríguez García:** Conceptualization; formal

analysis; investigation; methodology; writing – review and editing. **Juan-Luis Arsuaga:** Funding acquisition; project administration; resources; supervision; validation; writing – review and editing. **Rebeca García-González:** Conceptualization; formal analysis; investigation; methodology; writing – original draft; writing – review and editing.

## ACKNOWLEDGMENTS

We have benefitted from fruitful discussions with our colleagues from the Centro UCM-ISCIH sobre Evolución y Comportamiento Humanos of Madrid and the Laboratorio de Evolución Humana at the University of Burgos. Thanks to the anonymous reviewers of the manuscript for their valuable comments and suggestions that have helped us to improve the text. We thank our companions in the Atapuerca research and SH excavation team for their invaluable dedication to the ongoing work at the SH site. Thanks to Maria Cruz Ortega for her extraordinary and patient restoration of the fossils. Our acknowledgment and gratitude to Javier Trueba for the extraordinary graphic documentation of the SH fossils and fieldwork under very demanding conditions. The following individuals and their institutions for access to the recent and fossil comparative materials. P. Mennecier and A. Froment (Muséum National d'Histoire Naturelle); B. Maureille and C. Couture (Université de Bordeaux 1); Y. Haile-Selassie, B. Latimer, and L. Jellema (Cleveland Museum of Natural History); C. B. Stringer and R. Kruszynski (Natural History Museum, London); J. Radovčić (Croatian Natural History Museum); E. Cunha and A. L. Santos (Coimbra University) and A. Marcal (Bocage Museum). The fossils analyzed in this work are from the “Colección Museística de Castilla y León” of the Junta de Castilla y León.

## FUNDING INFORMATION

The Atapuerca research project is financed by Ministerio de Ciencia, Innovación y Universidades grant number PID2021-122355NB-C31 financed by MCIN/AEI/10.13039/501100011033/FEDER, UE. Fieldwork at the Atapuerca sites is funded by the Junta de Castilla y León and the Fundación Atapuerca.

## CONFLICT OF INTEREST STATEMENT

The authors declare no conflicts of interest.

## ORCID

José-Miguel Carretero  <https://orcid.org/0000-0003-0409-8087>

Rebeca García-González  <https://orcid.org/0000-0002-1035-6655>

Laura Rodríguez  <https://orcid.org/0000-0002-5090-1582>

## REFERENCES

- Aiello, L. C., & Dean, C. (1990). *An introduction to human evolutionary anatomy*. Academic Press.
- Alemseged, A., Spoor, F., Kimbel, W. H., Bobe, R., Geraads, D., Reed, D., & Wynn, J. G. (2006). A juvenile early hominin skeleton from Dikika, Ethiopia. *Nature*, *443*, 296–301.
- An, K. N., Morrey, B. F., & Chao, E. Y. S. (1983). Carrying angle of the human elbow joint. *Journal of Orthopaedic Research*, *1*(4), 369–378.
- Aranburu, A., Arsuaga, J. L., & Sala, N. (2017). The stratigraphy of the Sima de los Huesos (Atapuerca, Spain) and implications for the origin of the fossil hominin accumulation. *Quaternary International*, *433*(A), 5–21. <https://doi.org/10.1016/j.quaint.2015.02.044>
- Arsuaga, J. L., Carretero, J. M., Lorenzo, C., Gómez-Olivencia, A., Pablos, A., Rodríguez, L., García-González, R., Bonmatí, A., Quam, R. M., Pantoja-Pérez, A., Martínez, I., Aranburu, A., Gracia-Téllez, A., Poza-Rey, E., Sala, N., García, N., Alcázar de Velasco, A., Cuenca-Bescós, G., Bermúdez de Castro, J. M., & Carbonell, E. (2015). Postcranial morphology of the middle Pleistocene humans from Sima de los Huesos, Spain. *Proceedings of the National Academy of Sciences of the United States of America*, *112*, 11524–11529.
- Arsuaga, J. L., Carretero, J. M., Lorenzo, C., Gracia, A., Martínez, I., Bermúdez de Castro, J. M., & Carbonell, E. (1997). Size variation in middle Pleistocene humans. *Science*, *277*, 1086–1088.
- Arsuaga, J. L., Carretero, J. M., Martínez, I., & Gracia, A. (1991). Cranial remains and long bones from Atapuerca/Ibeas (Spain). *Journal of Human Evolution*, *20*(3), 191–230.
- Arsuaga, J. L., Lorenzo, C., Carretero, J. M., Gracia, A., Martínez, I., García, N., Bermúdez de Castro, J. M., & Carbonell, E. (1999). A complete human pelvis from the middle Pleistocene of Spain. *Nature*, *399*, 255–258.
- Arsuaga, J. L., Martínez, I., Arnold, L. J., Aranburu, A., Gracia-Téllez, A., Sharp, W. D., Quam, R., Falgueres, C., Pantoja-Pérez, A., Bischoff, J., Poza-Rey, E., Parés, J. M., Carretero, J. M., Demuro, M., Lorenzo, C., Sala, N., Martínón-Torres, M., García, N., Alcazar de Velasco, A., ... Carbonell, E. (2014). Neandertal roots: Cranial and chronological evidence from Sima de los Huesos. *Science*, *344*, 1358–1363.
- Auerbach, B. M., & Ruff, C. B. (2006). Limb bone bilateral asymmetry: Variability and commonality among modern humans. *Journal of Human Evolution*, *50*, 203–218.
- Basabe, J. M. (1966). El húmero premusteriense de Lezetxiki (Guipúzcoa). *Munibe. Sociedad de Ciencias Naturales Aranzadi (San Sebastian)*, *1*(4), 13–32.
- Bastir, M., García Martínez, D., Recheis, W., Barash, A., Coquerelle, M., Rios, L., Peña-Melian, A., García Río, F., & O'Higgins, P. (2013). Differential growth and development of the upper and lower human thorax. *PLoS One*, *8*, e75128.
- Beals, R. K. (1976). The normal carrying angle of the elbow. A radiographic study of 422 patients. *Clinical Orthopaedics and Related Research*, *119*, 194–196.
- Beiner, J. M., & Jokl, P. (2002). Muscle contusion injury and myositis Ossificans Traumatica. *Clinical Orthopaedics and Related Research*, *1976–2007*(403), S110–S119.
- Bermúdez de Castro, J. M., Carretero, J. M., García-González, R., Rodríguez-García, L., Martín-Torres, M., Rosell, J., Blasco, R., Martín-Francés, L., Modesto, M., & Carbonell, E. (2012). Early Pleistocene human humeri from the gran dolina-

- TD6 site (sierra de Atapuerca, Spain). *American Journal of Physical Anthropology*, 147, 604–617.
- Bermúdez de Castro, J. M., Martínez, I., Gracia-Téllez, A., Martínón-Torres, M., & Arsuaga, J. L. (2021). The Sima de los Huesos middle Pleistocene hominin site (Burgos, Spain). Estimation of the number of individuals. *The Anatomical Record*, 304(7), 1463–1477.
- Bonmatí, A., Gómez-Olivencia, A., Arsuaga, J. L., Carretero, J. M., Gracia, A., Martínez, I., Lorenzo, C., Bermúdez de Castro, J. M., & Carbonell, E. (2010). Middle Pleistocene lower back and pelvis from an aged human individual from the Sima de los Huesos site, Spain. *Proceedings of the National Academy of Sciences of the United States of America*, 107, 18386–18391.
- Boule, M. (1911). *L'Homme Fossile de La Chapelle aux Saints*. Masson et C.
- Brodeur, A. E., Silberstein, M. J., & Gravis, E. R. (1981). *Radiology of the pediatric elbow*. G.K. Hall.
- Buck, L. T., & Stringer, C. B. (2014). Homo heidelbergensis. *Current Biology*, 24(6), R214–R215.
- Cardoso, H. F. (2008). Age estimation of adolescent and young adult male and female skeletons II, epiphyseal union at the upper limb and scapular girdle in a modern Portuguese skeletal sample. *American Journal of Biological Anthropology*, 37(1), 97–105.
- Cardoso, H. F., Abrantes, J., & Humphrey, L. T. (2014). Age estimation of immature human skeletal remains from the diaphyseal length of the long bones in the postnatal period. *International Journal of Legal Medicine*, 128(5), 809–824.
- Carretero, J. M. (1994). *Estudio del esqueleto de las dos cinturas y el miembro superior de los homínidos de la Sima de los Huesos, Sierra de Atapuerca, Burgos [Tesis Doctoral]*. Universidad Complutense.
- Carretero, J. M., Arsuaga, J. L., Martínez, I., Quam, R., Lorenzo, C., Gracia, A., & Ortega Martínez, A. I. (2004). Los humanos de la Sima de los Huesos (Sierra de Atapuerca) y la evolución del cuerpo en el género Homo. In E. R. Baquedano, S. R. Jara, & E. A. Enríquez (Eds.), *Miscelanea en Homenaje a Emiliano Aguirre* (pp. 120–135). Museo Arqueológico Regional de Alcalá de Henares, Alcalá de Henares.
- Carretero, J. M., Haile-Selassie, Y., Rodríguez, L., & Arsuaga, J. L. (2009). A partial distal humerus from the Middle Pleistocene deposits at Bodo, Middle Awash, Ethiopia. *Anthropological Science*, 117, 19–31.
- Carretero, J. M., Lorenzo, C., & Arsuaga, J. L. (1997). Clavicles, scapulae and humeri from the Sima de los Huesos site (Sierra de Atapuerca, Spain). *Journal of Human Evolution*, 33(1–2), 357–348.
- Carretero, J. M., Lorenzo, C., & Arsuaga, J. L. (1999). Axial and appendicular skeleton of *Homo antecessor*. *Journal of Human Evolution*, 37(3–4), 459–499.
- Carretero, J. M., Rodríguez, L., García-González, R., Arsuaga, J. L., Gómez-Olivencia, A., Lorenzo, C., Bonmatí, A., Gracia, A., Martínez, I., & Quam, R. (2012). Stature estimation from complete long bones in the Middle Pleistocene humans from the Sima de los Huesos, Sierra de Atapuerca (Spain). *Journal of Human Evolution*, 62, 242–256.
- Carretero, J. M., Rodríguez, L., Quam, R. M., García-González, R., & Arsuaga, J. L. (2018). Exploring bone volume and skeletal weight in the Middle Pleistocene Humans from Sima de los Huesos Site (Sierra de Atapuerca, Spain). *Journal of Anatomy*, 233, 740–754.
- Chavaillon, J., Chavaillon, N., Coppens, Y., & Senut, B. (1977). Présence d'hominide dans le site Oldowayan de Gomboré I a Melka Kunturé, Ethiopie. *Comptes Rendus de l'Académie des Sciences*, 285(Serie D), 961–963.
- Churchill, S. E. (1996). Particulate versus integrated evolution of the upper body in late Pleistocene humans: A test of two models. *American Journal of Physical Anthropology*, 100, 559–583.
- Churchill, S. E. (1998). Cold adaptation, heterochrony, and Neandertals. *Evolutionary Anthropology*, 7(2), 46–60.
- Churchill, S. E., Holliday, T. W., Carlson, K. J., Jashashvili, T., Macias, M. E., Mathews, S., Sparling, T. L., Schmid, P., de Ruiter, D. J., & Berger, L. R. (2013). The upper limb of *Australopithecus sediba*. *Science*, 340, 1233477–1233477-5.
- Churchill, S. E., & Rhodes, J. A. (2009). The evolution of the human capacity for “killing at a distance”: The human fossil evidence for the evolution of projectile weaponry. In M. Richards & J. J. Hublin (Eds.), *The evolution of hominid diets: Integrating approaches to the study of Palaeolithic subsistence (Series: Vertebrate Paleobiology and Paleoanthropology)*. Springer.
- Churchill, S. E., & Trinkaus, E. (1990). Neandertal scapular glenoid morphology. *American Journal of Physical Anthropology*, 83, 147–160.
- Cowgill, L. (2007). Humeral torsion revisited: A functional and ontogenetic model for populational variation. *American Journal of Physical Anthropology*, 134, 472–480.
- Cushner, F. D., & Morwessel, R. M. (1992). Myositis ossificans traumatica. *Orthopaedic Review*, 21(11), 1319–1326.
- Delsaux, M. A. (1977). Les humérus fossiles. Comparaison avec les humérus modernes. *Bulletins et Mémoires de la Société d'Anthropologie de Paris*, 4, 165–175.
- Di Vincenzo, F., Churchill, S. E., & Manzi, G. (2012). The Vindija Neanderthal scapular glenoid fossa: Comparative shape analysis suggests evo-devo changes among Neanderthals. *Journal of Human Evolution*, 62(2), 274–285.
- Di Vincenzo, F., Rodríguez, L., Carretero, J. M., Collina, C., Geraads, D., Piperno, M., & Manzi, G. (2015). The massive fossil humerus from the Oldowan horizon of Gombore I, Melka Kunture (Ethiopia, >1.39 ma). *Quaternary Science Reviews*, 122, 207–221.
- Dittrick, J., & Suchey, J. M. (1986). Sex determination of prehistoric Central California skeletal remains using discriminant analysis of the femur and humerus. *American Journal of Physical Anthropology*, 70, 3–9.
- Edelson, G. (1999). Variations in the retroversion of the humeral head. *The Journal of Shoulder and Elbow Surgery*, 8(2), 142–145.
- Endo, B. (1971). Some characteristics of the deltoid tuberosity of the humerus in west-Asian and the European “classic” Neandertals. *The Anthropological Society of Nippon*, 79, 249–258.
- Endo, B., & Kimura, T. (1970). Postcranial skeleton of the Amud man. In H. Suzuki & F. Takai (Eds.), *The Amud man and his cave site*. The University of Tokyo.
- Feuerriegel, E. M., Green, D. J., Christopher, S., Walker, C. S., Peter Schmid, P., Hawks, J., Berger, L. R., & Churchill, S. E. (2017). The upper limb of homo Naledi. *Journal of Human Evolution*, 104, 155–173.
- Galtés, I., Jordana, X., Cos, M., Malgosa, A., & Manyosa, J. (2008). Biomechanical model of pronator efficiency: New insight into

- skeletal adaptation of the hominoid upper limb. *American Journal of Physical Anthropology*, 135, 293–300.
- García-González, R., Rodríguez, L., Salazar-Fernández, A., Arsuaga, J. L., & Carretero, J.-M. (2024). Updated study of adult and subadult pectoral girdle bones from Sima de los Huesos site (Sierra de Atapuerca, Burgos, Spain). Anatomical and age estimation keys. *The Anatomical Record*, 307(7), 2491–2518. <https://doi.org/10.1002/ar.25158>
- García-Martínez, D., Barash, A., Recheis, W., Utrilla, C., Torres-Sanchez, I., García-Rio, F., & Bastir, M. (2014). On the chest size of Kebara 2. *Journal of Human Evolution*, 70, 69–72.
- García-Martínez, D., Bastir, M., Gómez-Olivencia, A., Maureille, B., Golovanova, L., Doronichev, V., Akazawa, T., Osamu, K., Ishida, J., Gascho, D., Zollikofer, C. P. E., Ponce de León, M., & Heuzé, Y. (2020). Early development of the Neanderthal ribcage reveals a different body shape at birth compared to modern humans. *Science Advances*, 6(41), eabb4377.
- Gómez, M., Casado, A., Marina de Diego, M., Arias-Martorell, J., Pastor, J. F., & Potau, J. M. (2020). Quantitative shape analysis of the deltoid tuberosity of modern humans (*Homo sapiens*) and common chimpanzees (*pan troglodytes*). *Annals of Anatomy*, 230, 151505-3.
- Gómez-Olivencia, A., Barash, A., García-Martínez, D., Arlegi, M., Kramer, P., Bastir, M., & Been, E. (2018). 3D virtual reconstruction of the Kebara 2 Neandertal thorax. *Nature Communications*, 9, 4387.
- Gómez-Olivencia, A., Carretero, J. M., Arsuaga, J. L., Rodríguez, L., García-González, R., & Martínez, I. (2007). Metric and morphological study of the upper cervical spine from the Sima de los Huesos site (sierra de Atapuerca, Burgos, Spain). *Journal of Human Evolution*, 53(1), 6–25.
- Gómez-Olivencia, A., Eaves-Johnson, K. L., Franciscus, R. G., Carretero, J. M., & Arsuaga, J. L. (2009). Kebara 2: New insights regarding the most complete Neandertal thorax. *Journal of Human Evolution*, 57(1), 75–90.
- Heim, J. L. (1982). *Les Hommes fossiles de la Ferrassie*. Masson.
- Hublin, J. J. (2009). The origin of Neandertals. *Proceedings of the National Academy of Sciences of the United States of America*, 106(38), 16022–16027.
- Hublin, J. J., Tillier, A. M., & Tixier, J. (1987). L'humérus d'enfant moustérien (*Homo 4*) du Djebel Irhoud (Maroc) dans son contexte archéologique. *Bulletins et Mémoires de la Société d'Anthropologie de Paris*, 4(2), 115–141.
- Johnson, J. W., Thostenson, J. D., Suva, L. J., & Hasan, S. A. (2013). Relationship of bicipital groove rotation with humeral head retroversion. *Journal of Bone and Joint Surgery*, 95(8), 719–724.
- Kapandji, A. I. (1996). *Cuadernos de fisiología articular: Miembro Inferior*. Masson.
- Katzenberg, M. A., & Saunders, S. R. (2008). *Biological Anthropology of the Human Skeleton* (2nd ed.). Wiley.
- Konigsberg, L. W., Hens, S. M., Jantz, L. M., & Jungers, W. L. (1998). Stature estimation and calibration: Bayesian and maximum likelihood perspectives in physical anthropology. *American Journal of Physical Anthropology*, 107, 65–92.
- Krahl, V. E. (1976). The phylogeny and ontogeny of humeral torsion. *American Journal of Physical Anthropology*, 45(3), 595–599.
- Krogman, W. M., & Yasar-Iscan, M. (1986). *The human skeleton in forensic medicine*. Charles C. Thomas.
- Kronberg, M., Broström, L. A., & Söderlund, V. (1990). Retroversion of the humeral head in the normal shoulder and its relationship to the normal range of motion. *Clinical Orthopaedics and Related Research*, 253, 113–117.
- Kuhn, J. E. (2016). Throwing, the shoulder, and human evolution. *The American Journal of Orthopedics*, 45(3), 110–114.
- Kumar, B., Pai, S., Ray, B., Mishra, S., Siddaraju, K. S., Pandey, A. K., & Binu, S. (2010). Radiographic study of carrying angle and morphometry of skeletal elements of human elbow. *Romanian Journal of Morphology and Embryology*, 51(3), 521–526.
- Larsen, C. S. (1997). *Bioarchaeology: Interpreting behavior from the human skeleton*. Cambridge University Press.
- Larsen, C. S., Ruff, C. B., & Kelly, R. L. (1995). Structural analysis of the Stillwater postcranial human remains: Behavioral implications of articular joint pathology and long bone diaphyseal morphology. *Anthropological Papers of the AMNH*, 77, 107–133.
- Larson, S. G. (2007a). The definition of humeral torsion: A comment on Rhodes (2006). *American Journal of Physical Anthropology*, 133, 819–820.
- Larson, S. G. (2007b). Evolutionary transformation of the hominin shoulder. *Evolutionary Anthropology*, 16, 172–187.
- Larson, S. G. (2009). Evolution of the hominin shoulder: Early *homo*. In F. E. Grine, J. G. Fleagle, & R. E. Leakey (Eds.), *The first humans—Origin and early evolution of the genus homo: Contributions from the third stony brook human evolution symposium and workshop October 3–October 7, 2006* (pp. 65–75). Springer.
- Larson, S. G. (2015). Humeral torsion and throwing proficiency in early human evolution. *Journal of Human Evolution*, 85, 198–205.
- Larson, S. G., Jungers, W. L., Morwood, M., Sutikna, T., Jatmiko, Saptomo, E. W., Due, R. A., & Djubiantono, T. (2007). *Homo floresiensis* and the evolution of the hominin shoulder. *Journal of Human Evolution*, 53(6), 718–731.
- Larson, S. G., Jungers, W. L., Tocheri, M. W., Orr, C. M., Morwood, M. J., Sutikna, T., Rokhus, D. A., & Djubiantono, T. (2009). Descriptions of the upper limb skeleton of *Homo floresiensis*. *Journal of Human Evolution*, 57(5), 555–570.
- Leijnse, J. N. A. L., Han, S. H., & Kwon, Y. H. (2008). Morphology of deltoid origin and end tendons a generic model. *Journal of Anatomy*, 213, 733–742.
- Lieberman, D. E., Devlin, M. J., & Pearson, O. M. (2001). Articular area response to mechanical loading effects of exercise, age and skeletal location. *American Journal of Physical Anthropology*, 116, 266–277.
- Lordkipanidze, D., Jashashvili, T., Vekua, A., Ponce de Leon, M. S., Zollikofer, C. P. E., Rightmire, G. P., Pontzer, H., Ferring, R., Oms, O., Tappen, M., Bukhsianidze, M., Agusti, J., Kahlke, R., Kiladze, G., Martínez-Navarro, B., Mouskhelishvili, A., Nioradze, M., & Rook, L. (2007). Postcranial evidence from early *Homo* from Dmanisi, Georgia. *Nature*, 449, 305–309.
- Lorenzo, C., Carretero, J. M., Arsuaga, J. L., Gracia, A., & Martínez, I. (1998). Intrapopulation body size variation and cranial capacity variation in middle Pleistocene humans: The Sima de los Huesos sample (sierra de Atapuerca, Spain). *American Journal of Physical Anthropology*, 106, 19–33.
- Lovejoy, C. O., Johanson, D. C., & Coppens, Y. (1982). Hominid upper limb bones recovered from the Hadar formation:

- 1974-1977 collections. *American Journal of Physical Anthropology*, 57, 637-650.
- Lovejoy, C. O., Simpson, S. W., White, T. D., Asfaw, B., & Suwa, G. (2009). Careful climbing in the Miocene: The forelimbs of *Ardipithecus ramidus* and humans are primitive. *Science*, 326(5949), 70-78.
- Lozano, M., Mosquera, M., Bermúdez de Castro, J. M., Arsuaga, J. L., & Carbonell, E. (2009). Right handedness of *Homo heidelbergensis* from Sima de los Huesos (Atapuerca, Spain) 500,000 years ago. *Evolution and Human Behavior*, 30(5), 369-376.
- Manzi, G. (2011). Before the emergence of *Homo sapiens*: Overview on the early-to-middle Pleistocene fossil record (with a proposal about *Homo heidelbergensis* at the subspecific level). *International Journal of Evolutionary Biology*, 2011, 582678.
- Martin, R., & Saller, K. (1928). *Lehrbuch der Anthropologie. Band II. Kranilogie. Osteologie*. Gustav Fischer Verlag.
- McCown, T., & Keith, A. (1939). *The stone age of Mount Carmel. Vol. 2, The fossil human remains from the Levalloio-Mousterian*. Oxford.
- Melillo, S., Gunz, P., Coqueugniot, H., Reske, S., & Hublin, J. J. (2019). Structural effects of variation in the human clavicle. *American Journal of Physical Anthropology*, 168, 687-704.
- Modesto-Mata, M., García-González, R., Quintino, Y., García-Campos, C., Martínez de Pinillos, M., Martín-Francés, L., Martínón-Torres, M., Heuzé, Y., Carbonell, E., Arsuaga, J. L., Dean, C., & Bermúdez de Castro, J. M. (2022). Early and middle Pleistocene hominins from Atapuerca (Spain) show differences in dental developmental patterns. *American Journal of Biological Anthropology*, 178(2), 273-285.
- Mounier, A., Marchal, F., & Condemi, S. (2009). Is *Homo heidelbergensis* a distinct species? New insight on the Mauer mandible. *Journal of Human Evolution*, 56(3), 219-246.
- Paraskevas, G., Papadopoulos, A., Papaziogas, B., Spanidou, S., Argiriadou, H., & Gigis, J. (2004). Study of the carrying angle of the human elbow joint in full extension: A morphometric analysis. *Surgical and Radiologic Anatomy*, 26, 19-23.
- Patil, S., Sethi, M., & Vasudeva, N. (2016). Determining angle of humeral torsion using image software technique. *Journal of Clinical and Diagnostic Research*, 10(10), AC06.
- Pérez-Criado, L., Rosas, A., Bastir, M., & Pastor, J. F. (2017). Humeral laterality in modern humans and Neanderthals: A 3D geometric morphometric analysis. *Anthropological Science*, 125(3), 117-128.
- Poza-Rey, E. M., Lozano, M., & Arsuaga, J. L. (2017). Brain asymmetries and handedness in the specimens from the Sima de los Huesos site (Atapuerca, Spain). *Quaternary International*, 433, 32-44.
- Rhodes, J. A. (2007). Humeral torsion and retroversion in literature: A reply to Larson. *American Journal of Physical Anthropology*, 133, 820-821.
- Rhodes, J. A., & Churchill, S. E. (2009). Throwing in the middle and upper Paleolithic: Inferences from an analysis of humeral retroversion. *Journal of Human Evolution*, 56, 1-10.
- Roach, N. T., & Lieberman, D. E. (2014). Upper body contributions to power generation during rapid, overhand throwing in humans. *The Journal of Experimental Biology*, 217, 2139-2149.
- Roach, N. T., Lieberman, D. E., Gill, T. J., Palmer, W. E., & Gill, T. J. (2012). The effect of humeral torsion on rotational range of motion in the shoulder and throwing performance. *Journal of Anatomy*, 220, 293-301.
- Roach, N. T., & Richmond, B. G. (2015). Humeral torsion does not dictate shoulder position, but does influence throwing speed. *Journal of Human Evolution*, 85, 206-211.
- Roach, N. T., Venkadesan, M., Rainbow, M. J., & Lieberman, D. E. (2013). Elastic energy storage in the shoulder and the evolution of high-speed throwing in homo. *Nature*, 498, 483-486.
- Rodríguez, L. (2013). *Estudio biomecánico de los huesos largos del esqueleto apendicular de los homínidos del Pleistoceno Medio de la Sima de los Huesos, Sierra de Atapuerca (Burgos): implicaciones paleobiológicas y filogenéticas [PhD thesis]*. University of Burgos.
- Rosas, A., Martínez-Maza, C., Bastir, M., García-Taberner, A., Lalueza-Fox, C., Huguet, R., Ortiz, J. E., Juliá, R., Soler, V., de Tores, T., Martínez, E., Cañaveras, J. C., Sánchez-Moral, S., Cuezva, S., Lario, J., Santamaría, D., de la Rasilla, M., & Fortea, J. (2006). Paleobiology and comparative morphology of a late Neandertal sample from El Sidron, Asturias, Spain. *Proceedings of the National Academy of Sciences of the United States of America*, 103, 19266-19271.
- Rosas, A., Pérez-Criado, L., Bastir, M., Estalrich, A., Huguet, R., García-Taberner, A., Pastor, J. F., & de la Rasilla, M. (2015). A geometric morphometrics comparative analysis of Neandertal humeri (epiphyses-fused) from the El Sidrón cave site (Asturias, Spain). *Journal of Human Evolution*, 82, 51-66.
- Ruff, C. B. (2000). Body size, body shape, and long bone strength in modern humans. *Journal of Human Evolution*, 38, 269-290.
- Ruff, C. B. (2008). Biomechanical analyses of archaeological human skeletons. In M. A. Katzenberg & S. R. Saunders (Eds.), *Biological anthropology of the human skeleton* (2nd ed., pp. 183-206). Wiley.
- Ruff, C. B., Trinkaus, E., Walker, A., & Larsen, C. S. (1993). Postcranial robusticity in homo. I: Temporal trends and mechanical interpretation. *American Journal of Physical Anthropology*, 91, 21-53.
- Senut, B. (1981). *L'Humerus et ses articulations chez les Homínidés Plio-Pleistocènes*. Centre National de la Recherche Scientifique.
- Shang, H., Tong, H., Zhang, S., Chen, F., & Trinkaus, E. (2007). An early modern human from Tianyuan cave, Zhoukoudian, China. *Proceedings of the National Academy of Sciences of the United States of America*, 104(16), 6573-6578.
- Shang, H., & Trinkaus, E. (2010). *The early modern human from Tianyuan cave, China*. Texas A&M University Press.
- Shaw, C. N., Hofmann, C. L., Petraglia, M. D., Stock, J. T., & Gottschall, J. S. (2012). Neandertal Humeri may reflect adaptation to scraping tasks, but not spear thrusting. *PLoS One*, 7(7), e40349. <https://doi.org/10.1371/journal.pone.0040349>
- Sládek, V., Ruff, C. B., Berner, M., Holt, B., Niskanen, M., Schuplerová, E., & Hora, M. (2016). The impact of subsistence changes on humeral bilateral asymmetry in terminal Pleistocene and Holocene Europe. *Journal of Human Evolution*, 92, 37-49.
- Smith, F. (1976). *The neandertal remains from Krapina: A descriptive and comparative study [PhD Thesis]*. University of Michigan.
- Steel, F. L. D., & Tomlinson, J. D. W. (1958). The carrying angle in man. *Journal of Anatomy*, 92, 315-317.

- Stern, J. T., Jr., & Susman, R. L. (1983). The locomotor anatomy of *Australopithecus afarensis*. *American Journal of Physical Anthropology*, 60, 279–317.
- Stringer, C. B. (2012). The status of *Homo heidelbergensis* (Schoetensack 1908). *Evolutionary Anthropology*, 21, 101–107.
- Tattersall, I. (2011). Before the Neanderthals: Hominid evolution in middle Pleistocene Europe. In *Continuity and discontinuity in the peopling of Europe* (pp. 47–53). Springer.
- Themido, A. A. (1926). Sobre alguns caracteres sexuais dos húmeros portugueses. *Revista da Universidade de Coimbra*, X, 1-4, 104–173.
- Thoma, A. (1975). Were the spy fossils evolutionary intermediates between classic neanderthal and modern man? *Journal of Human Evolution*, 4, 387–410.
- Trinkaus, E. (1983). *The Shanidar Neanderthals*. Academic Press.
- Trinkaus, E., & Churchill, S. E. (1999). Diaphyseal cross-sectional geometry of near eastern middle Palaeolithic humans: The Humerus. *Journal of Archaeological Science*, 26, 173–184.
- Trinkaus, E., Churchill, S. E., & Ruff, C. B. (1994). Postcranial robusticity in homo. II: Humeral bilateral asymmetry and bone plasticity. *American Journal of Physical Anthropology*, 93, 1–34.
- Trinkaus, E., Churchill, S. E., Ruff, C. B., & Vandermeersch, B. (1999). Long bone shaft Robusticity and body proportions of the Saint-Césaire 1 Châtelperronian Neanderthal. *Journal of Archaeological Science*, 26(7), 753–773.
- Vandermeersch, B. (1991). La ceinture scapulaire et les membres supérieurs. In *Le Squelette Mousterien de Kebara 2. Cahiers de Paleanthropologie* (pp. 157–178). CNRS, Paris.
- Vandermeersch, B., & Trinkaus, E. (1995). The postcranial remains of the Régourdou 1 Neanderthal: The shoulder and arm remains. *Journal of Human Evolution*, 28, 439–476.
- Voisin, J. (2006). Clavicle, a neglected bone: Morphology and relation to arm movements and shoulder architecture in primates. *Anatomical Record Part A*, 288, 944–953.
- Walker, A., & Leakey, R. E. F. (1993). *The Nariokotome Homo erectus skeleton*. Springer.
- White, T. D., Suwa, G., & Asfaw, B. (1994). *Australopithecus ramidus*, a new species of early hominid from Aramis, Ethiopia. *Nature*, 371(6495), 306–312.
- Yokley, T. R., & Churchill, S. E. (2006). Archaic and modern human distal humeral morphology. *Journal of Human Evolution*, 51(6), 603–616.

**How to cite this article:** Carretero, J.-M., García-González, R., Rodríguez, L., & Arsuaga, J.-L. (2024). Main anatomical characteristics of the hominin fossil humeri from the Sima de los Huesos Middle Pleistocene site, Sierra de Atapuerca, Burgos, Spain: An update. *The Anatomical Record*, 307(7), 2519–2549. <https://doi.org/10.1002/ar.25194>